Lithos, 26 (1990) 67–98
Elsevier Science Publishers B.V., Amsterdam

Alkaline igneous rocks of Magnet Cove, Arkansas: Mineralogy and geochemistry of syenites

Marta J.K. Flohr and Malcolm Ross
U.S. Geological Survey, M.S. 959, Reston, VA 22092 (U.S.A.)

(Received December 19, 1989; accepted April 12, 1990)

LITHOS

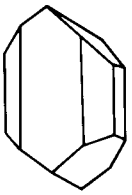

ABSTRACT

Flohr, M.J.K. and Ross, M., 1990. Alkaline igneous rocks of Magnet Cove, Arkansas: Mineralogy and geochemistry of syenites. In: A.R. Woolley and M. Ross (Editors), Alkaline igneous rocks and carbonatites. Lithos, 26: 67–98.

Syenites from the Magnet Cove alkaline igneous complex form a diverse mineralogical and geochemical suite. Compositional zoning in primary and late-stage minerals indicates complex, multi-stage crystallization and replacement histories. Residual magmatic fluids, rich in F, Cl, CO_2 and H_2O, reacted with primary minerals to form complex intergrowths of minerals such as rinkite, fluorite, V-bearing magnetite, F-bearing garnet and aegirine. Abundant sodalite and natrolite formed in pegmatitic segregations within nepheline syenite where Cl- and Na-rich fluids were trapped. During autometasomatism compatible elements such as Mn, Ti, V and Zr were redistributed on a local scale and concentrated in late-stage minerals. Early crystallization of apatite and perovskite controlled the compatible behavior of P and Ti, respectively. The formation of melanite garnet also affected the behaviour of Ti, as well as Zr, Hf and the heavy rare-earth elements. Pseudoleucite syenite and garnet–nepheline syenite differentiated along separate trends, but the two groups are related to the same parental magma by early fractionation of leucite, the presumed precursor of intergrowths of K-feldspar and nepheline. The Diamond Jo nepheline syenite group defines a different differentiation trend. Sphene–nepheline syenite, alkali syenite and several miscellaneous nepheline syenites do not consistently plot with the other syenite groups or each other on element and oxide variation diagrams, indicating that they were derived from still other parental syenite magmas. Mineral assemblages indicate that relatively high f_{O_2}, at or above the fayalite–magnetite–quartz buffer, prevailed throughout the crystallization history of the syenites.

Introduction

The Magnet Cove complex is a 101-Ma (Zartman, 1977; Eby, 1987) alkaline ring-dike complex that crops out over an area of approximately 12 km^2 in Hot Spring County, Arkansas. Areas of Ti, V and Nb mineralization are found both within the complex and in country rock adjacent to it (e.g., Erickson and Blade, 1963 and references therein).

One purpose of our study of Magnet Cove is to better characterize the mineralization process(es), as to the source(s) of the elements of interest and the transport mechanism(s). To address these questions, it is important to understand how various minor and trace elements behave throughout the crystallization histories of the igneous rocks and also during late metasomatic or hydrothermal stages. A detailed petrographic and electron microprobe study was undertaken to characterize the syenites and the behaviour of various elements. Whole-rock major-, minor- and trace-element compositions were also obtained on selected samples. Analytical methods are the same as those described by Flohr and Ross (1989). A second purpose of our study of Magnet Cove is to investigate the genetic relationships among the different rock units. Data from a diverse suite of syenites are presented in this paper.

0024-4937/90/$03.50

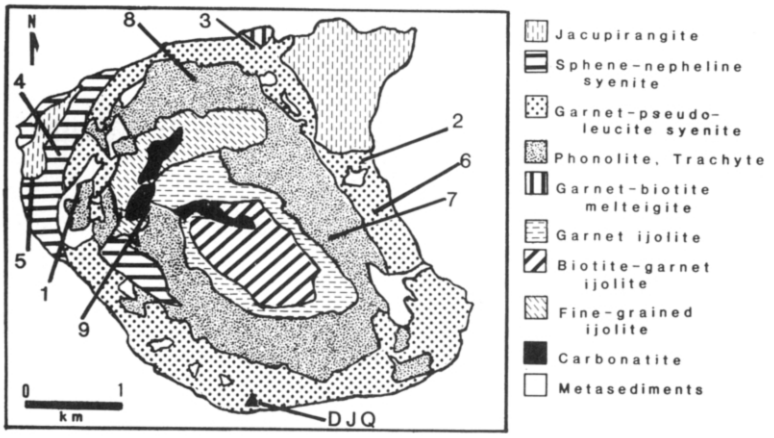

Fig. 1. Geological map of the Magnet Cove complex, from Erickson and Blade (1963). *DJQ*=Diamond Jo quarry. Samples discussed in the text are from the following localities: (*1*) pseudoleucite syenite 84-25A, 83-32; (*2*) garnet–nepheline syenite 86-55, pseudoleucite syenite 86-55B; (*3*) garnet–nepheline syenite 86-60; (*4*) sphene–nepheline syenite 86-59, 85-15B; (*5*) nepheline syenite 86-64; (*6*) nepheline syenite 85-17; (*7*) nepheline syenite 86-56A, 85-14B; (*8*) nepheline syenite 86-62B; (*9*) nepheline syenite 84-20. (*DJQ*) Diamond Jo nepheline syenite 2-DJ7, 1-DJ8, 2-DJ10, 3-DJ10, 5-DJ10, 1B-100, 2-098, 2-100, 2-157; pseudoleucite syenite 1-DJ11; garnet–nepheline syenite 4-DJ10, 1-71A, 1-157, 3-157, 83-31, A-DJ10; alkali syenite 83-51.

Geological setting

The first detailed petrographic study and geological map of the Magnet Cove complex were made by Williams (1891). Erickson and Blade (1963) remapped the complex and provided a detailed geochemical study of the major lithologies. The reader is referred to the study of Erickson and Blade for a detailed description of the geology of the complex and age relationships of the rock units. The units shown in Fig. 1 are as designated by Erickson and Blade (1963). The geology of Magnet Cove is, however, much more complex than is indicated by this map. For example, a variety of syenites are found within the garnet–pseudoleucite syenite unit and small outcrops of syenites and felsic and mafic dikes are found in the unit of phonolite and trachyte. Exposures of fresh syenite are rare.

The best exposures of coarse-grained nepheline syenite, pseudoleucite syenite and garnet–nepheline syenite are found at the Diamond Jo quarry. Located in the southern part of the Magnet Cove complex, this quarry was mapped in detail by Owens and Howard (1991, in press). Here, xenoliths of ijolite and metamorphosed country rock are abundant in pseudoleucite syenite and garnet–nepheline syenite. The textures and mineral compositions of the ijolite xenoliths were described by Flohr and Ross (1989). Sample locations of syenites and xenoliths we collected from the quarry are shown in fig. 2 of Flohr and Ross (1989). Locations of samples we collected outside the quarry are shown in Fig. 1 of this paper.

Syenite groups and general textural observations

The outer ring of the Magnet Cove complex consists of a variety of syenites that we group as follows: (1) Diamond Jo nepheline syenite, (2) pseudoleucite syenite, (3) garnet–nepheline syenite, which includes slightly more mafic rocks that are modally malignites, (4) sphene–nepheline syenite, (5) alkali syenite and (6) miscellaneous nepheline syenites. Some of these designations are consistent with the map units of Erickson and Blade (1963), but others are not.

Diamond Jo nepheline syenite is uniformly coarse-grained and was mapped by Erickson and Blade (1963) as "nepheline syenite pegmatite". All of our samples of this syenite were collected from Diamond Jo quarry. The coarse grain size, trace-element characteristics (such as the high Ba and Sr concentrations noted by Erickson and Blade) and very Fe-rich mafic minerals serve to distinguish this syenite from the other syenites.

Rocks from our next two syenite groups, pseudoleucite syenite and garnet–nepheline syenite, were collected from the unit mapped by Erickson and Blade (1963) as "garnet–pseudoleucite syenite".

They noted the heterogeneous nature of the "garnet–pseudoleucite syenite" and the absence of pseudoleucite in parts of the unit. In this paper, we refer to syenite from Erickson and Blade's "garnet–pseudoleucite syenite" unit as pseudoleucite syenite if it contains pseudoleucite and garnet–nepheline syenite if it does not. Pseudoleucite syenite is further distinguished from garnet–nepheline syenite by trace-element characteristics.

Modal data (T. Armbrustmacher; written commun., 1985 and visual estimates of modes) indicate that samples of garnet-nepheline syenite range from relatively mafic nepheline syenite to malignite (using the classification system of Sørensen, 1974, table 2). However, for the sake of simplicity and because modal, textural and chemical continua exist we collectively refer to all modal varieties as garnet–nepheline syenite.

Textural comparisons between various samples of garnet–nepheline syenite are further complicated by mafic segregations. These segregations consist of different proportions of green pyroxene laths, biotite and anhedral melanite garnet, with minor amounts of interstitial K-feldspar and nepheline. They are mineralogically like their host rock, although their average grain size is significantly smaller. The segregations have rounded to scalloped margins and some have diffuse margins. The segregations do not appear to be partly reacted xenoliths as the textures and mineral compositions are distinct from those of ijolite or country rock xenoliths.

The contact between pseudoleucite syenite and garnet–nepheline syenite is distinct in hand sample because of the presence or absence of pseudoleucite. No chill zone or reaction zone was observed at the contact. However, because the groundmass of pseudoleucite syenite is texturally and mineralogically similar to that of garnet–nepheline syenite, the contact between the two types of syenites appears gradational in thin section.

Sphene–nepheline syenite, our fourth syenite group, was collected from the sphene–nepheline syenite unit of Erickson and Blade (1963). This syenite contains amphibole-rich mafic segregations. The mineralogy of the segregations is similar to that of their host rocks although their average grain size is smaller.

Alkali syenite, our fifth syenite group, was collected from the rim of Diamond Jo quarry, near the country rock contact. Contacts between alkali syenite and the other syenites exposed at the quarry were not found. Alkali syenite is the most evolved rock described in this paper and its mineralogy is distinct.

Our sixth syenite group, miscellaneous nepheline syenites, includes samples from the outer syenite ring and from small outcrops of nepheline syenite within the unit mapped by Erickson and Blade (1963; Fig. 1) as undivided phonolite and trachyte. These nepheline syenites are chemically and/or mineralogically distinct from each other and from syenites of the five groups described above.

Whole-rock chemistry

Almost all nepheline syenites (Table 1) from Magnet Cove are chemically and mineralogically intermediate between agpaitic and miaskitic syenites. (See Sørenson (1974) for the chemical and mineralogical characteristics used to classify nepheline syenites as agpaitic or miaskitic.) For example, the Diamond Jo nepheline syenites have agpaitic indices [defined as the molecular proportions of (Na_2O+K_2O) to Al_2O_3] of 1 or slightly >1, low MgO and $Fe_2O_3 > FeO$ (Table 1). However, unlike agpaitic syenites, Diamond Jo nepheline syenites have low concentrations of Zr, Nb, U, Th, Zn and the rare-earth elements (REE) and relatively high concentrations of CaO. The presence of rinkite, fluorite, melanite, biotite and magnetite also indicates an intermediate position between agpaitic and miaskitic syenites. Sphene–nepheline syenite 86-59 and nepheline syenite 86-56A are miaskitic in character.

Major and minor elements

Syenites from Magnet Cove, considered as a whole, form generally well-defined trends on most Harker diagrams (Fig. 2). Fe^{3+}, Fe^{2+}, Mg, Ca, Ti and P behave as compatible elements, whereas Al and K behave as incompatible elements. The trend for Mn is ill defined, but Mn values are higher in the more mafic syenites than in the more felsic ones. Na shows no correlation with SiO_2. Chlorine is high in Diamond Jo nepheline syenites, sphene–nepheline syenite, and nepheline syenites 86-64 and 86-62B relative to the other syenites (Fig. 2k). Fluorine data (Fig. 2l) show considerable scatter and

TABLE 1

Whole-rock major-, minor- and trace-element data from syenites

Locality+	Diamond Jo nepheline syenite							Pseudoleucite syenite			Alkali syenite
Sample	DJQ 2-DJ10	DJQ 1B-100	DJQ 1-DJ8	DJQ 5-DJ10	DJQ 2-098	DJQ 2-DJ7	DJQ 2-100	1 84-25A	DJQ 1-DJ11	2 86-55B	DJQ 83-51
wt.%											
SiO_2	54.0	52.7	52.3	52.1	51.8	51.2	49.8	52.5	51.2	46.9	61.6
TiO_2	0.17	0.38	0.18	0.26	0.11	0 20	0.36	0.26	0.36	0.94	0.24
Al_2O_3	21.5	16.8	21.0	20.8	22.2	19.1	20.5	20.4	21.4	19 7	17.0
Fe_2O_3	1 9	3.4	2.2	2.9	1.8	2 8	3.7	2.3*	2.0	4.0*	2.1*
FeO	0.80	1.8	0.80	1.2	0.90	1.7	1.9	1.20	1.50	2.21	0.44
MnO	0 17	0.40	0.21	0.27	0.18	0.35	0.35	0.30	0.18	0.29	0.12
MgO	0.17	0.66	0.23	0.38	0.29	0.60	0.43	0.29	0.45	0.91	0.36
CaO	1.6	6.1	2.2	3.0	1.9	4.4	4.3	2.15	3.0	7.18	1.23
Na_2O	7.5	5.7	8.3	8.5	8.9	7.6	9.0	4.64	6.9	6.04	2.67
K_2O	8.5	7.7	8.3	7.8	8.2	7.3	6.6	9.61	9.3	7.09	11.7
P_2O_5	0.06	0.08	0.07	0.07	0 07	0.08	0.10	0.07	0.12	0.23	0.05
$H_2O^@$	0.87	1.18	1 16	1.16	0.91	1.19	1.25	3.38	1.50	1.87	1.10
CO_2	0.97	1.7	1.3	1 1	1.2	1.6	1.1	1.70	1.20	1 24	0.04
Cl	0 20	0.15	0.25	0.32	0.28	0.23	0.17	0.025	0.030	0.060	0.047
F	0.11	0.22	0.24	0.22	0.20	0.21	0.21	0.079	0.170	0.020	0.086
S	0.14	0.22	0.17	0.22	0.26	0.17	0.16	0.14	0.11	0 04	0.050
Sum	98.66	99.19	98.91	100.3	99.20	98.73	99.93	99.04	99.42	98.72	98.83
(Na_2O+K_2O) $/Al_2O_3$**	1.00	1.05	1.08	1.08	1.06	1.07	1.07	0.884	1.00	0 894	1 00

ppm											
La	39.3	51.3	54 1	57.9	50.1	51.3	83.6	107	53.8	48.4	36#
Ce	44.4	77.0	65.0	76.5	59.8	67.0	107	107 3	67.5	75.5	65.8
Nd	5.9	13.3	9.3	10.7	7.3	8.7	15.9	13.4	9.4	20.9	14
Sm	0 46	1.15	0.63	0.88	0.52	0.58	1.11	1.03	0.97	2.5	1.95
Eu	0.101	0.288	0.150	0.193	0.120	0.110	0.248	0.244	0.228	0.625	0.427
Tb	0.115	0.168	0.088	0.150	0 139	0.225	0 180	0.242	0.147	0 307	0.316
Yb	0 43	0.61	0 46	0.62	<0.4	0 43	0.46	0.48	0.49	1 01	0.96
Lu	0 059	0.089	0.048	0.051	<0.07	<0.08	0.055	0.072	0.090	0.161	0.138
Ba	11100	17000	5210	4470	9600	13900	5730	2440	2750	822	6000
Rb	233	215	244	188	212	203	188	494	598	411	305
Sr	4190	4380	4430	3450	4050	3750	2860	2030	1750	1160	1830
Nb	45	55	71	96	31	67	122	118	90	72	43
Ta	1.84	2.46	2.74	3.22	1.47	2.32	3 91	3.02	2.81	3.48	1.42
Zr	114	130	98	152	72	138	189	158	157	212	171
Hf	0.87	1.06	0.70	1.20	0.48	1.02	1.54	1.20	1.49	2.53	3.00
Y	<2	<2	<2	<2	<2	<2	<2	5	7	7	6
Th	4 50	6.74	4.12	6.42	3.83	6.48	8.20	7.48	4.01	3.38	5 53
U	2.20	2.10	2.74	3.88	1.61	2.54	3.57	4.85	2.60	2.23	2.04
Sc	0.062	0.113	0.047	0.253	0.049	0.069	0 106	0.162	0.271	0.361	1.012
V	60	180	74	140	54	80	200	81	130	530	67
Cr	7.2	3.4	2.9	3.2	2.2	2 6	4.0	2 8	2.8	7.0	7
Co	0 92	4.21	1.17	2.23	1.44	2.34	2 62	1.27	2.37	4.73	1.91
Ni	<32	<40	<30	<40	<30	<40	<40	<40	<40	<50	<40
Cu	5	10	7.6	10	16	15	12	3 3	20	<3	5
Zn	75	82	64	106	54	138	104	128	85	71	50
Sb	1 61	2.80	1.23	49	1.70	6.05	1 80	1.83	0.49	0.106	0 560
Cs	2.15	1.54	1.99	2.71	2.24	1.83	2.11	5.75	16.6	10.31	3.39
Pb	7	9	10	180	11	48	7	35	8	<5	9
Rb/Sr	0.056	0.049	0.055	0.054	0.052	0.054	0.066	0.243	0 342	0.354	0.167
Nb/Ta	24.5	22.3	25.9	29.8	21.1	28.9	31.2	39.1	32.0	20.7	30.3
Zr/Hf	131	123	140	127	150	135	122	132	105	83.8	57.0
Th/U	2.04	3.21	1.50	1.65	2.38	2.55	2.30	1.54	1 54	1.52	2.71

TABLE 1 (continued)

Locality+ Sample	Garnet–nepheline syenite						Sph.–neph. syenite	Miscellaneous nepheline syenites			
	3 86-60	DJQ 3-157	DJQ 1-17A	DJQ 1-157	DJQ 4-DJ10	2 86-55	4 86-59	5 86-64	6 85-17	7 86-56A	8 86-62B
wt.%											
SiO_2	49.0	46.8	46.1	45 0	44 9	42.2	46 4	53.6	49.9	49.8	49.1
TiO_2	0.75	0.97	0.89	1.20	1.30	1.91	3.01	0.20	0.56	1.52	0.71
Al_2O_3	19.4	19.5	17.4	18.0	19.7	16.8	15.7	21.6	20.1	20.2	19.5
Fe_2O_3	4 8*	4.7	4 6*	6.0	5 2	6.5*	3.9*	2.5*	4 3*	2.0*	3.2*
FeO	1.6	2.6	4.3	2.8	2.7	3.8	5.7	1.6	1.4	4.6	2.04
MnO	0.41	0.33	0.54	0.42	0.36	0.45	0.27	0.27	0 33	0.32	0.33
MgO	0.77	1.0	1 4	1.2	1.2	2.03	3.14	0.30	0.47	1.31	0 58
CaO	5.31	7.4	8.82	9.0	8.3	12.7	9.76	2.26	4 34	6.53	3.78
Na_2O	7.42	7.4	7.91	7.5	7 9	5.95	5.32	7.90	6.52	6.16	7.67
K_2O	6.60	6.1	5.4	4.9	6.3	4.32	3.51	7.88	7 60	4 75	7.57
P_2O_5	0.16	0.28	0.38	0.28	0.27	0.51	0.68	0.050	0.08	0.26	0.09
$H_2O^@$	1.96	1.30	1.10	1.97	1.11	1.94	1.36	0.64	1.76	1.10	1.08
CO_2	1.00	0.72	0.33	1.00	0.46	1.10	0.10	0.07	0.63	0.10	2.02
Cl	0.055	0.070	0.024	0.029	0.03	0 041	0.340	0.500	<0.010	0.008	0.44
F	0.16	0.28	0.32	0.24	0.23	0.13	0.25	0.012	0.11	0.25	0.14
S	0.038	0.23	0.12	0 19	0.13	0.041	0.27	0.10	0.03	1.20	0.47
Sum	99.43	99.68	99.63	99.73	100.1	100.4	99.71	99.48	98 13	100.1	98 72
(Na_2O+K_2O) $/Al_2O_3$**	0.997	0.963	1.08	0.980	1.01	0.861	0.799	0.997	0.943	0.756	1.07

ppm											
La	74.4	58.5	89.7	67.7	52.8	72.1	166	6.12	82.6	93.7	89.9
Ce	95	73	115	96	79	109	284	12.3	99	121	114.8
Nd	17.1	17.2	24	19.9	21	30	98	<12	13.7	38.2	22.1
Sm	1.79	2.56	2.66	2 9	3.14	4.92	17	0.54	1.23	6.1	2.58
Eu	0.463	0.66	0.623	0.841	0.950	1.545	4.32	0.099	0.277	1.67	0.707
Tb	0.293	0.40	0 38	0.53	0.54	0.90	1.74	0.057	0.189	0 82	0.54
Yb	0 77	1.66	1.17	2.63	2.28	3.86	3.8	0.34	<0.8	2.82	1.19
Lu	0.120	0.251	0.156	0.393	0.332	0.54	0 507	<0.05	0 06	0.388	0.157
Ba	2780	3320	1320	1910	1100	531	1580	2360	6460	2080	3080
Rb	273	279	264	158	306	225	124	184	322	161	334
Sr	2550	1890	2050	2080	1590	1470	1730	1260	2850	2610	2290
Nb	154	133	162	105	112	116	213	59	175	200	174
Ta	4.49	3.81	4 05	3.43	4 05	5 02	16	2 30	4.53	6.94	4.80
Zr	271	310	287	329	334	401	389	95	207	407	396
Hf	2 53	3.00	2.63	3.59	3.60	4.67	8.3	0.84	1.85	5.55	4.61
Y	<2	11	8	16	17	24	23	<2	<2	15	6
Th	7.54	4 97	6.88	4.61	4.36	4.02	19 3	1 23	7.41	8.60	18.0
U	4.12	3.31	4 16	3.62	3 09	2.80	4.63	4.65	5.91	3 30	8.04
Sc	0.42	0.493	0.880	0.523	0.301	0.790	7.03	0.093	0.112	1.540	0.418
V	300	460	590	610	660	840	300	76	410	280	250
Cr	3.1	2.5	<5	4 2	5.0	3 1	12.7	<3	9.4	5.8	8.2
Co	4.44	5.50	7.40	5.99	6.40	11.9	22 6	1.84	3.51	8.00	5.75
Ni	<50	na	<60	na	na	<60	<70	<40	<50	<50	<60
Cu	4.3	12	8.3	7.5	8.8	10	32	6	<3	10	5
Zn	21	106	166	113	129	103	143	145	163	151	218
Sb	0.25	1.03	0.36	0 42	0.41	0 099	1 12	<0.1	1.16	0 261	1.74
Cs	3 87	7.22	2.95	2 52	8.32	7 12	2.97	2.80	7.31	0 92	11 3
Pb	14	9	13	5	14	6	10	<5	11	13	47
Rb/Sr	0 107	0.148	0 129	0.076	0.192	0.153	0 072	0 146	0.113	0.062	0 146
Nb/Ta	34.3	34.9	40.0	30.6	27.6	23.1	13 3	25.7	38.6	28.8	36.3
Zr/Hf	107	103	110	91.6	92.2	85.9	46 8	114	112	73 3	85.9
Th/U	1.83	1.50	1.65	1.27	1 41	1.44	4.17	0.265	1.25	2.61	2.25

Major oxides, excluding FeO,determined by ICP-AES (inductively coupled plasma-atomic emission spectroscopy) by M Kavulak, J. Marinenko and N. Rait in syenites from Diamond Jo quarry and by X-ray fluorescence by J. Taggart, A. Bartel and E. Robb in all other syenites. FeO, H_2O, CO_2, S, F and Cl determined by various techniques by E. Brandt, H. Christie, J Sharkey, L. Jackson, H. Smith, C Skeen, H. Kirschenbaum and R. Moore. Ba, Rb, Sr, Nb, Y and Zr determined by EDS XRF (energy-dispersive X-ray fluorescence) by J. Evans. V, Cu and Pb determined by atomic absorption by M. Doughten. All other elements determined by INAA (instrumental neutron activation analysis) by G. Wandless and J. Mee. $^{+}$DJQ=Diamond Jo quarry; locality numbers are keyed to Fig. 1. *Fe_2O_3 calculated from total Fe obtained as Fe_2O_3 and reported FeO. $^{@}$Total H_2O reported. **Molecular proportions. #La not reported by INAA for sample 83-51, reported value obtained by EDS XRF.

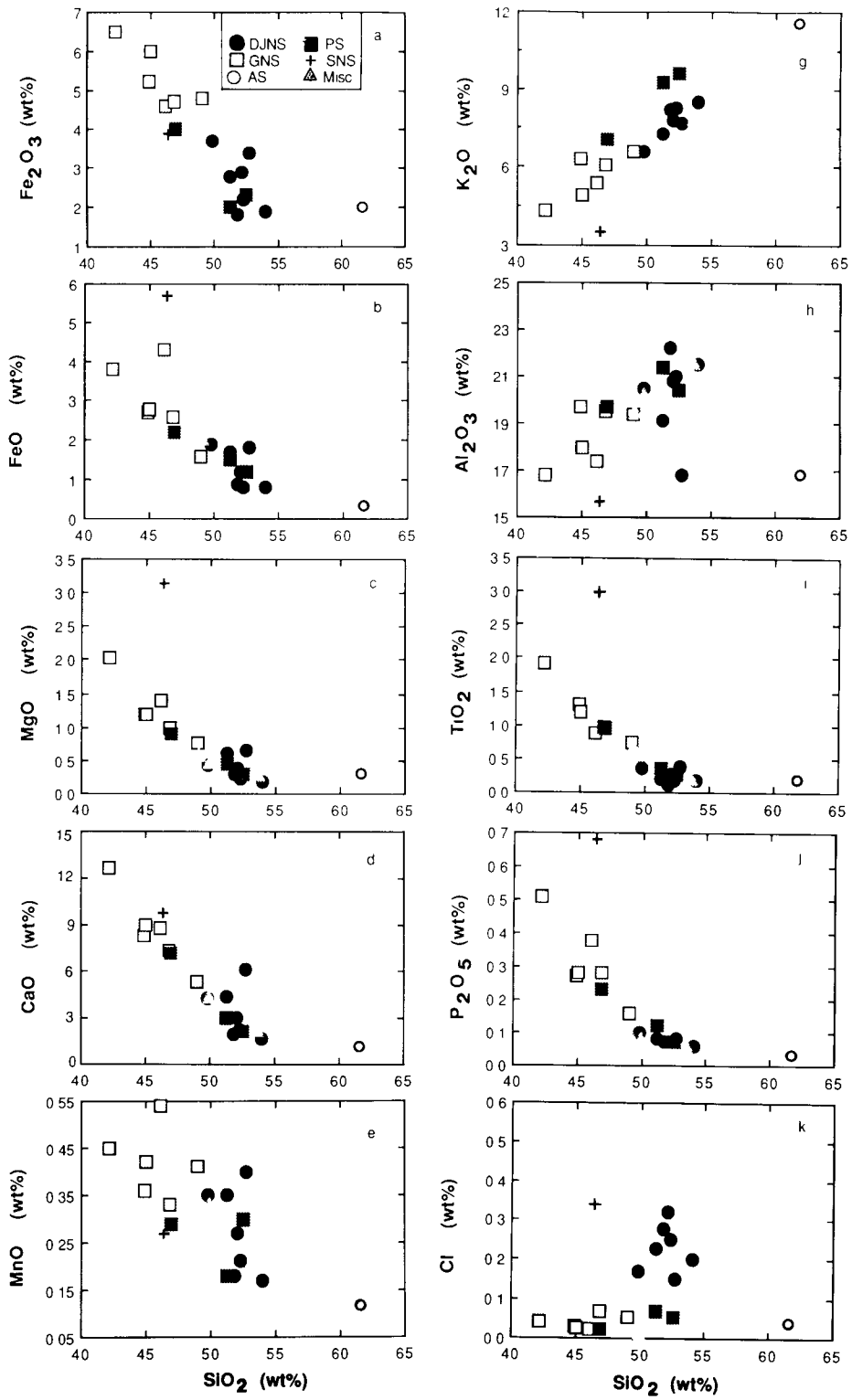

Fig. 2. Oxide (a–j) and halogen (k, l) variation (Harker) diagrams for syenites from the Magnet Cove complex. Abbreviations are as follows: DJNS – Diamond Jo nepheline syenite; PS – pseudoleucite syenite; GNS – garnet–nepheline syenite; SNS – sphene–nepheline syenite; AS – alkali syenite; Misc. – miscellaneous nepheline syenites. Symbol key for all plots given in plot a.

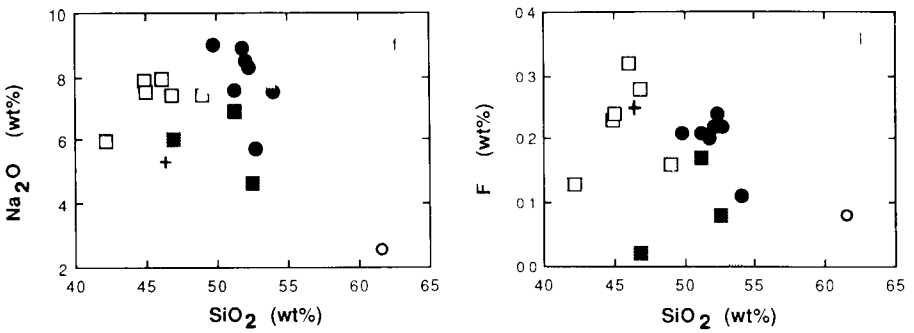

Fig. 2. (continued)

no clear correlation with SiO_2. H_2O and CO_2 have overall ranges of 0.64–3.38 wt.% and 0.04–2.02 wt.%, respectively (Table 1). Miaskitic sphene–nepheline syenite 86-59 and nepheline syenite 86-56A commonly fall off the defined trends. The most mafic pseudoleucite syenite (86-55B) plots with garnet–nepheline syenite. Alkali syenite 83-51 is the most silica-rich syenite analyzed and, with the exception of its K_2O and MnO contents, consistently falls off the trends defined by the other rocks.

Trace elements

Syenites from Magnet Cove have a range of REE concentrations (Table 1) and REE patterns (Fig. 3) that are broadly similar. All the syenites are enriched in the light REE (LREE) relative to the heavy REE (HREE). Diamond Jo nepheline syenite samples show very steep slopes from La to Eu and have low concentrations of the middle REE (MREE) to HREE (Fig. 3a). Pseudoleucite syenite and garnet–nepheline syenite (Fig. 3b, c) also have steep slopes in LREE to MREE, but most samples are richer in the MREE and HREE than is Diamond Jo nepheline syenite. The inconsistent development of pronounced negative Eu anomalies in only some samples of Diamond Jo nepheline syenite and one sample of pseudoleucite syenite (Fig. 3a, b) is puzzling and inexplicable at this time. Sphene–nepheline syenite 86-59 and nepheline syenite 86-56A have the highest REE concentrations and have similar, slightly concave REE patterns (Fig. 3d). Nepheline syenite 86-64 is depleted in total REE and has a distinct REE pattern (Fig. 3d) compared to the other syenites (Fig. 3a–d).

Nd, Sm, Eu and Tb behave as compatible elements, whereas La and Ce do not show any consistent relationship when plotted against SiO_2 (not shown). All the syenites, except for the two miaskitic syenites and alkali syenite, define good linear trends on plots of Nd, Sm, Eu and Tb vs. SiO_2. Yb, Lu and Y are uniformly low in samples of Diamond Jo nepheline syenite and behave as compatible elements in the other syenites, except the three noted above for Nd, Sm, Eu and Tb.

Sr, Rb and Ba generally behave as incompatible elements. Diamond Jo nepheline syenite, garnet–nepheline syenite and pseudoleucite syenite each define a different trend on the Sr-, Rb- and Ba–SiO_2 and Sr–Rb plots (Fig. 4a–d) and also on the K–Rb plot (not shown). Sphene–nepheline syenite, alkali syenite and miscellaneous nepheline syenites do not consistently plot with any of the other groups (Fig. 4). Diamond Jo nepheline syenite is characterized by very high concentrations of Ba and Sr and pseudoleucite syenite by high concentrations of Rb (as well as Cs, Table 1).

Diamond Jo nepheline syenite, pseudoleucite syenite and garnet–nepheline syenite are further distinguished by other trace-element characteristics. Zr/Hf of Diamond Jo nepheline syenite is higher than that of garnet-nepheline syenite (Table 1); Zr/Hf of pseudoleucite syenite is lower than or overlaps with that of Diamond Jo nepheline syenite and garnet–nepheline syenite. Samples of Diamond Jo nepheline syenite have a range of Th/U and an average of 2.23, which is significantly higher than the average Th/U of pseudoleucite syenite (1.53) and garnet–nepheline syenite (1.52). There is overlap in Nb/Ta (Table 1) among the three aforementioned groups.

Despite differences in Zr/Hf (Table 1), a good

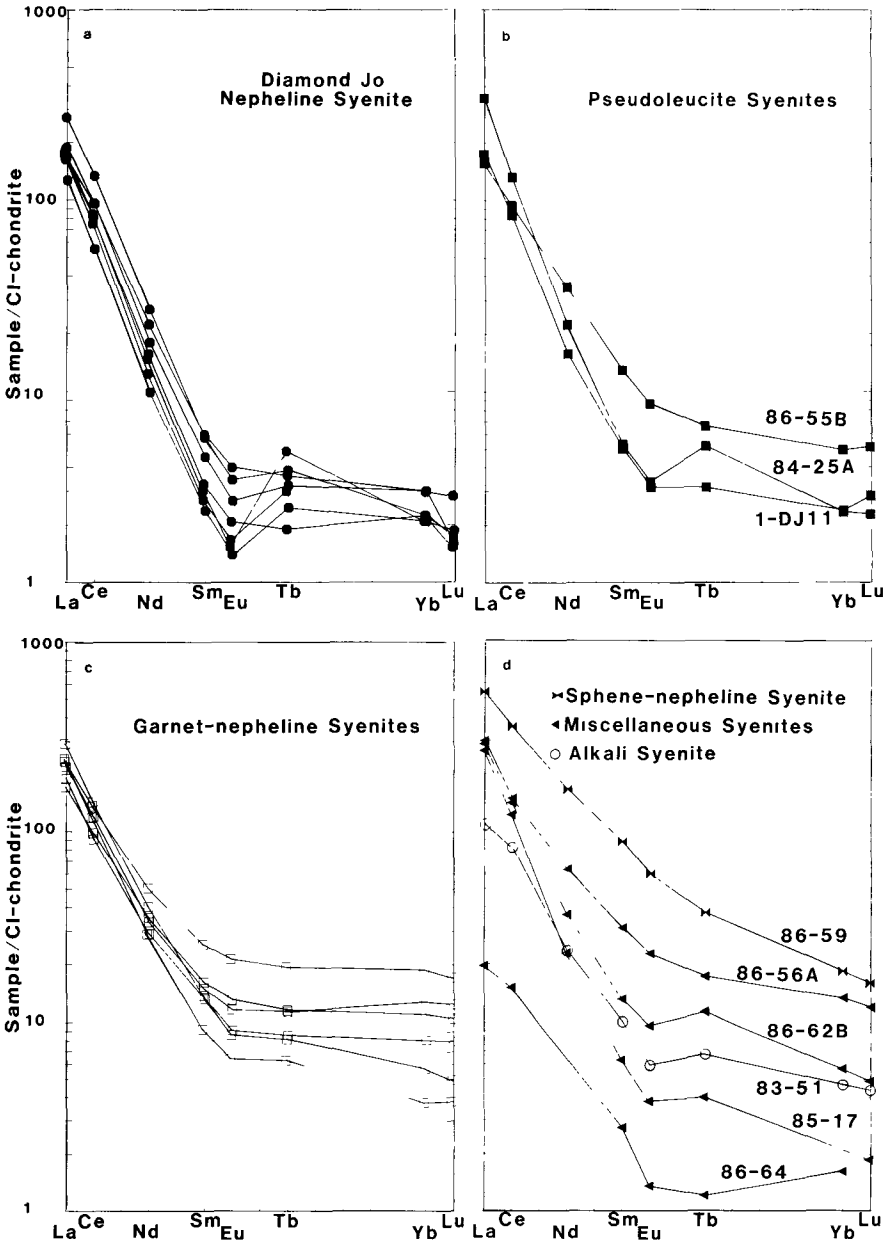

Fig. 3. CI-chondrite normalized rare earth element data for syenites from the Magnet Cove complex.

positive linear relationship exists between Zr and Hf when all syenites are considered (Fig. 5); only sphene–nepheline syenite and alkali syenite fall off the trend. Ti, V and Zr are generally positively correlated with one another within the syenite suite (Table 1). The relationship between TiO_2 and V is shown (Fig. 6) as an example. The following generalizations can be made regarding the behavior of various trace elements. Zr, Hf and Co behave as compatible elements when plotted against SiO_2. Th, Nb and V show good compatible behavior in the garnet–nepheline syenite and pseudoleucite syenite groups, but no trends are defined by samples of Diamond Jo nepheline syenite.

Alkali syenite 83-51, sphene–nepheline syenite 86-59 and the miscellaneous nepheline syenites do not have trace-element characteristics that allow them to be consistently grouped with Diamond Jo nepheline syenite, garnet–nepheline syenite, or pseudoleucite syenite (Table 1; Figs. 5, 6).

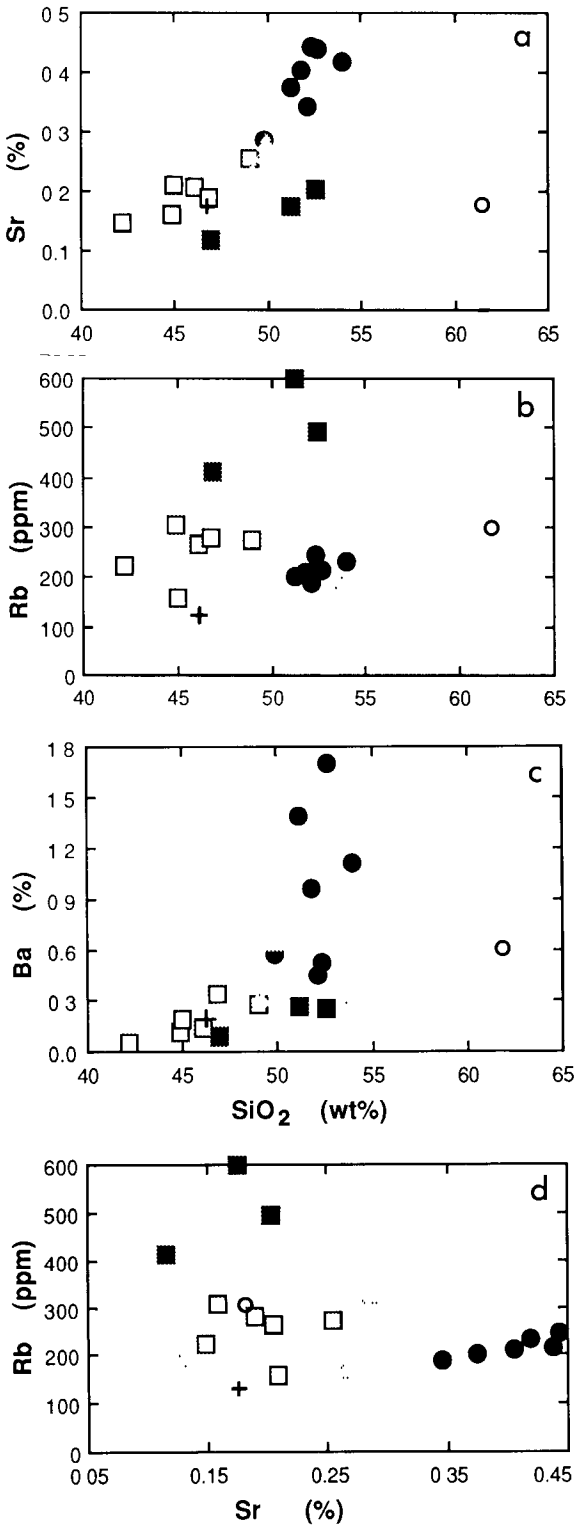

Fig. 4. Sr, Rb and Ba variation diagrams for syenites from the Magnet Cove complex. Samples from pseudoleucite syenite, garnet–nepheline syenite and Diamond Jo nepheline syenite define separate trends. Symbols as in Fig. 2a.

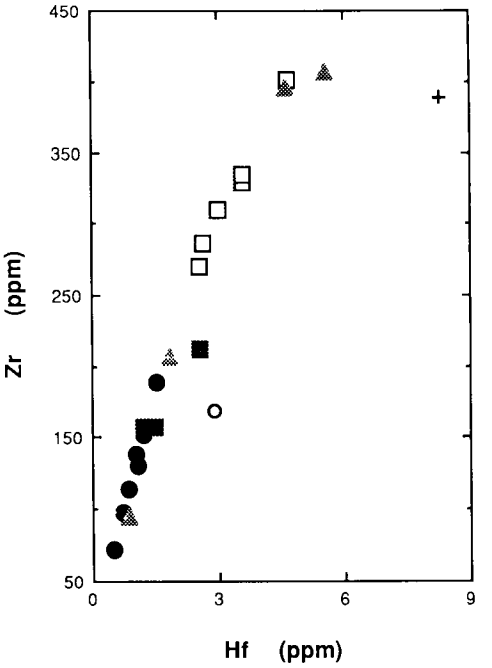

Fig. 5. Zr–Hf variation diagram for syenites from the Magnet Cove Complex. Both Zr and Hf have higher concentrations in the more mafic garnet-nepheline syenites and sphene-nepheline syenite than in Diamond Jo nepheline syenites and pseudoleucite syenites. Symbols as in Fig. 2a.

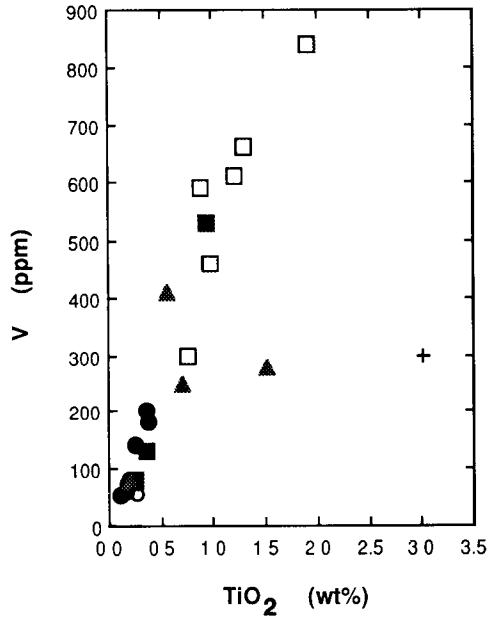

Fig. 6. V–TiO_2 variation diagram for syenites from the Magnet Cove complex. Garnet–nepheline syenites, with relatively abundant melanite garnet, contain more Ti and V than do the more felsic syenites. Symbols as in Fig. 2a.

Pb and Sb are rather low in all samples except 5-DJ10. The Pb-isotope systematics of a K-feldspar separate from 5-DJ10 are not anomalous when compared with those from two other samples of Diamond Jo nepheline syenite (R. Ayuso, pers. commun., 1988). The high values of Pb and Sb in 5-DJ10 compared with other samples (Table 1) suggest the presence of a mineral such as galena, although such a phase has not been identified in thin section.

Petrographic descriptions and mineral compositions

Diamond Jo nepheline syenite

Diamond Jo nepheline syenite is coarse- to medium-grained with a hypidiomorphic texture. K-feldspar is the most abundant mineral. Textural relationships indicate the following crystallization sequences: magnetite + hedenbergite + nepheline; hedenbergite + nepheline + melanite garnet; nepheline + melanite garnet + aegirine-augite. K-feldspar was the last primary mineral to crystallize; it includes grains of nepheline, hedenbergite and melanite but never aegirine-augite. Acicular to tabular wollastonite is the most common inclusion found within feldspar in some samples, but it is absent in others. Nepheline is partly replaced by cancrinite and minor amounts of aegirine. Rare natrolite and sodalite crystallized interstitially to feldspar laths.

K-feldspar (Fig. 7a) is zoned, with higher Ba and lower K in the cores relative to the rims (Table 2, no. 1, 2). Oscillatory zoning of Ba and K is also observed. Ba-rich grains are mantled by and, in some samples, extensively or completely replaced by microperthitic, brown, inclusion-rich K-feldspar (Table 2, no. 3). The Ba-rich and Ba-poor feldspars are optically distinct and the contact between them is abrupt.

Hedenbergite is partly resorbed and mantled by aegirine-augite (Table 3, no. 1, 2). The hedenber-

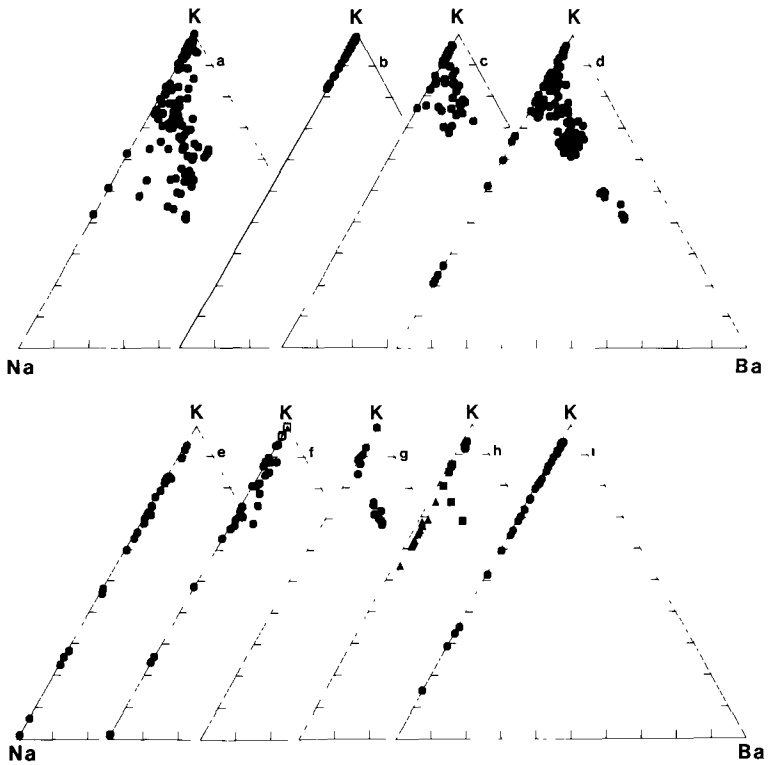

Fig. 7. Electron microprobe analyses of alkali feldspars plotted in the system K–Na–Ba (cations). (a) Diamond Jo nepheline syenite; (b, c) feldspar within pseudoleucites and in the groundmass surrounding pseudoleucites, respectively, from pseudoleucite syenites; (d) garnet–nepheline syenites; (e) sphene–nepheline syenite; (f) alkali syenite (filled hexagons) and grains within vugs (open squares) of alkali syenite; (g) nepheline syenite 85-17; (h) nepheline syenites 84-20 (filled hexagons), 86-62B (filled squares), 85-14B (filled triangles); (i) nepheline syenite 86-64.

TABLE 2

Representative compositions of feldspar from syenites

Sample	Diamond Jo nepheline syenite			Pseudoleucite syenite	Garnet–nepheline syenite		Sphene–nepheline syenite		Alkali syenite
	3-DJ10			86-55	A-DJ10		85-15B		83-51
	1	2	3	4	5	6	7	8	9
wt.%									
SiO_2	58.5	62.5	64.9	65.1	47.2	55.9	60.7	65 4	68.5
Al_2O_3	20.8	19.9	18.7	18.8	23.7	21.0	25.2	19.1	19.3
FeO	0.51	0.34	0 26	0.05	0.35	0.40	0.20	0.12	0.35
MgO	0.02	0 02	nd	nd	nd	nd	0 03	0.04	nd
CaO	0 05	0.04	nd	0 02	0 12	0 07	5 97	0.08	nd
BaO	7.29	3 53	0.17	nd	19 9	9.76	0 16	0 35	nd
Na_2O	1.72	2 03	0.67	0.73	1.23	1 50	7.90	2 02	11.6
K_2O	11.0	12.4	15.6	15 8	5 82	9 76	0 30	13 6	0.21
Sum	99.89	100.76	100 30	100 50	98.32	98.39	100.46	100.71	99 96
Cations									
Si	2.825	2.911	2.986	2 988	2 525	2.780	2 690	2.978	2.998
Al	1.180	1 091	1 017	1.017	1.495	1.230	1.318	1.028	0 994
	4.005	4.002	4 003	4.005	4.020	4.010	4 008	4.005	3 992
Fe	0.021	0.013	0.010	0.002	0.016	0.017	0.007	0 005	0.013
Mg	0 001	0.001	0	0	0	0	0 002	0 003	0
Ca	0.003	0 002	0	0.001	0 007	0.004	0 283	0 004	0
Ba	0.138	0 064	0.003	0	0.418	0 190	0.003	0.006	0
Na	0 161	0 183	0.060	0 065	0.128	0 145	0.679	0 178	0.989
K	0 674	0.737	0 916	0 925	0 397	0.619	0 017	0 794	0.012
	0.998	1.000	0.989	0.994	0.966	0.975	0.991	0.990	1.014
Molecular proportions									
Ab	16.5	18.5	6.1	6.5	13 4	15 1	69.1	18.2	98 8
An	0.3	0.2	0	0 1	0 7	0 3	28 9	0.4	0.
Or	69.1	74 8	93.6	93 4	41.8	64.7	1 7	80.8	1 2
Cn	14.1	6 5	0.3	0	44 0	19 9	0 3	0 6	0
No. pts. averaged	3	3	3	7	4	4	5	3	3

Cations calculated per 8 oxygens, nd = not detected; Ab = albite; An = anorthite; Or = orthoclase; Cn = celsian. Columns are as follows: 1 to 3–Core, rim, and overgrowth, respectively, 4–Grain within pseudoleucite, 5, 6–Perthitic intergrowth of two Ba-rich feldspars (Fig. 10b, c), 7, 8–Andesine and K-feldspar overgrowth, respectively, 9–Albite rim on K-feldspar

gite cores of the composite grains are continuously zoned with outwardly decreasing Al and Mg and increasing Si and Fe. The aegirine-augite mantles are zoned with Fe^{3+}, Na and Si increasing and Mg, Al, Ti and Fe^{2+} decreasing outward to the rims of these overgrowths. Commonly, overgrowths of Ti- and Al-rich aegirine discontinuously rim the aegirine-augite. In some samples, hedenbergite is completely replaced by aegirine-augite and, where replacement is even more extensive, aegirine-augite is replaced by aegirine (Table 3, no. 4) with accessory ilmenite (Table 4, no. 13) or ilmenite plus magnetite.

Pyroxenes are enriched in Na with progressive crystallization (Fig. 8a). Hedenbergite cores cluster in a small area of the plot, whereas aegirine-augites and aegirines form a continuous trend when data from several crystals are considered. Individual grains, however, show only limited zoning in the more sodic part of the plot.

Red melanite garnet is commonly intergrown with hedenbergite and is zoned, with Ti decreasing from core to rim (Table 5, no. 1, 2). The cation substi-

TABLE 3

Representative compositions of pyroxene from syenites

Sample	Diamond Jo nepheline syenite				Garnet–nepheline syenite			
	2-DJ7		2-DJ7	2-157	83-31	83-31		86-60
	1	2	3	4	5	6	7	8
wt.%								
SiO_2	48.5	51.2	52.4	51 7	43.6	42.3	50.1	51.2
TiO_2	0 53	0 32	2.34	1.79	3.44	1.85	0.48	0.33
ZrO_2	nd	nd	nd	0.46	na	na	na	0.02
Al_2O_3	1.93	1.10	0.67	1.35	8.53	9 53	1.15	0.85
V_2O_3	nd	nd	nd	0.22	na	na	na	0.33
Fe_2O_3*	6.75	17.7	29.3	24.2	6.78	7.26	8.39	19.1
FeO*	14.0	12.2	1.06	4.87	2.36	7.39	11.8	9.04
MnO	1.60	1 54	1.09	0.93	0 14	0.51	1.50	1.30
MgO	5.07	0.04	0.04	0 38	11 6	6.81	5.44	1.17
CaO	20.3	8.77	0.61	1.62	23.5	22.6	18.5	9.46
Na_2O	1.69	7.86	13.3	11.9	0.43	0.71	2 90	7.96
Sum	100.37	100.73	100.81	99 42	100.38	98.96	100.26	100.76
Cations								
Si	1.904	2.001	1 989	1.998	1.635	1.648	1.949	1.986
Al	0.089	0	0.011	0.002	0.365	0.352	0.051	0.014
	1.994	2.001	2.000	2.000	2.000	2.000	2.000	2.000
Al	0	0.051	0.019	0.059	0.011	0.085	0.001	0.025
Ti	0.016	0.009	0.067	0.052	0.097	0.054	0.014	0.010
Zr	0	0	0	0.010	–	–	–	0
V	0	0	0	0.007	–	–	–	0 010
Fe^{3+}	0.198	0.522	0.838	0 704	0.191	0.213	0.246	0.558
Fe^{2+}	0.458	0.398	0.034	0.157	0.074	0.241	0.382	0.293
Mn	0.037	0.018	0.035	0	0	0.013	0.042	0.036
Mg	0.297	0.002	0.002	0.011	0.627	0.395	0.315	0.068
	1.006	1.000	0.995	1.000	1.000	1.001	1.000	1.000
Mn	0.016	0.033	0	0 030	0.004	0.004	0.007	0 007
Mg	0	0	0	0.011	0 020	0	0	0
Ca	0.855	0.368	0.025	0.067	0.945	0.942	0.771	0.393
Na	0.129	0.596	0.980	0.892	0.031	0.054	0.219	0.600
	1.000	0.997	1.005	1.000	1.000	1.000	0.997	1.000
No. pts. averaged	3	3	5	8	3	3	3	3

tutions observed in melanite from Magnet Cove syenites are like those found in melanite from ijolite xenoliths (Flohr and Ross, 1989).

Some melanite is marginally replaced by aegirine or by aegirine intergrown with pyrrhotite and minor calcite. Extensive replacement of melanite and hedenbergite by complex intergrowths of rinkite, fluorite, calcite, magnetite, sphene and birefringent garnet, which is compositionally similar to fluorohydrograndite from ijolite xenoliths (Flohr and Ross, 1989), is also common.

Four different occurrences of magnetite are observed in Diamond Jo nepheline syenite. Type I magnetite (Table 4, no. 1, 2) crystallized early, whereas Types II, III and IV (Table 4, no. 3, 4, 5) are found in replacement assemblages. Type II magnetite occurs as small, anhedral grains intergrown with biotite (Table 6, no. 1) that replace pyroxene. In the Type II magnetites, Ti is positively correlated with Mn and the Mn contents of coexisting magnetite and biotite are positively correlated. Type III magnetite is intergrown with aegirine and Mn- and Nb-rich ilmenite (Table 4, no. 12) and replaces aegirine-augite. Type IV magnetite is inter-

TABLE 3 (continued)

Sample	Sphene–neph. syenite		Miscellaneous nepheline syenites					
	85-15B		85-17	84-20		85-14B		86-64
	9	10	11	12	13	14	15	16
wt.%								
SiO_2	47.8	50.0	51 0	51.3	51.9	47 1	46.5	49.0
TiO_2	1.80	0.40	0.30	0.38	1.17	1 84	0.78	0.40
ZrO_2	0.06	0.05	nd	0.04	nd	0.02	0.14	0 07
Al_2O_3	5.13	2.47	1.24	0 77	0 67	5.53	4 22	1.38
V_2O_3	0.06	0.04	0.14	0.17	0.06	0.03	0 11	0.07
Fe_2O_3*	5 24	5 27	12.9	10.8	31.6	5.94	8.25	11.3
FeO*	6.37	9.92	6 21	7.41	0	3.63	9.86	12.7
MnO	0.46	0.63	1.67	0 76	0 66	0.58	1.31	2 34
MgO	10.3	8 59	6.52	7.81	0.36	11 8	6.44	2.90
CaO	22.3	21.5	15.7	17 6	0 57	21.9	21.0	16.8
Na_2O	1.09	1.46	4.67	3 65	13.4	1.01	1.48	3.71
Sum	100.61	100 33	100.35	100.69	100.39	99.35	100.09	100.67
Cations								
Si	1.799	1.910	1.949	1 948	1 973	1.777	1.811	1.929
Al	0.201	0.090	0.051	0.034	0.027	0.223	0.189	0.064
	2 000	2.000	2.000	1.983	2.000	2.000	2.000	1.993
Al	0.026	0 021	0.005	0	0.003	0 022	0.004	0
Ti	0 051	0 011	0 009	0.011	0 033	0 052	0.023	0.012
Zr	0.001	0.001	0	0.001	0	0	0.003	0 002
V	0.002	0.001	0.004	0.005	0.002	0.001	0 003	0.002
Fe^{3+}	0.148	0.152	0.371	0.310	0.905	0.169	0.242	0.333
Fe^{2+}	0.200	0.317	0.198	0.235	0	0.114	0.321	0.418
Mn	0	0.008	0.042	0.011	0.021	0	0.030	0.070
Mg	0.572	0.489	0.371	0 443	0 020	0.642	0.374	0 170
	1.000	1.000	1 000	1.016	0 984	1 000	1 000	1.007
Mn	0.015	0.012	0.012	0 013	0	0.019	0.013	0 008
Mg	0.006	0	0	0	0	0.022	0	0
Ca	0 899	0.880	0 642	0.718	0 023	0 885	0 875	0.709
Na	0.080	0.108	0.346	0.269	0 992	0 074	0.112	0.283
	1.000	1.000	1.000	1.000	1.015	1.000	1.000	1.000
No. pts. averaged	5	3	3	4	5	8	6	7

nd = not detected; na = not analyzed. Columns are as follows: 1, 2–Discontinuously zoned grain with a core of hedenbergite and a rim of aegirine-augite, respectively; 3–Aegirine laths, with a range of 1.31–3.44 wt.% TiO_2, that form rosettes in a groundmass of natrolite and sodalite; 4–Aegirine intergrown with magnetite and ilmenite (Table 4, no. 4, 12), 5–Pleochroic pink core of diopside that is discontinuously zoned to a rim of aegirine-augite (rim is similar in composition to no. 7, this table); 6, 7–Discontinuously zoned grain with core of diopside and rim of aegirine-augite, 8–Aegirine-augite lath; 9, 10–Core and rim, respectively, of discontinuously zoned diopside; 11–Relatively Mg-rich aegirine-augite; 12, 13–Aegirine-augite from nepheline syenite and aegirine that occurs with natrolite from pegmatite, respectively; 14, 15–Diopside phenocryst and anhedral groundmass hedenbergite, respectively; 16–Anhedral groundmass grains. *Fe^{2+} and Fe^{3+} calculated by assuming ideal stoichiometry of 4 cations per 6 oxygens.

grown with rinkite, fluorite, aegirine, colourless garnet and calcite and contains significant V.

The most metasomatized nepheline syenite studied is one of several pegmatitic segregations within Diamond Jo nepheline syenite sample 2-DJ7. The groundmass consists of abundant sodalite, natrolite, aegirine, a mineral tentatively identified as spodiophyllite (Table 7, no. 2; the composition is sim-

TABLE 4

Representative compositions of oxides from syenites

Sample	Diamond Jo nepheline syenite					Pseudoleucite syenite		Gar–neph. syenite	Sph.–neph. syenite	Miscell. nepheline syenites		Diamond Jo neph. syenite		Alkali syenite	Gar–neph. syenite
	Magnetite											Ilmenite		Anatase	Perovskite
	2-157		2-100	2-157	5-DJ10	83-32		86-60	85-15B	85-14B	86-64	2-157	2-DJ7	83-51	3-157
	1	2	3	4	5	6	7	8	9	10	11	12	13	14	15
wt.%															
SiO_2	nd	0.03	0.07	0.07	0.16	0.11	0.15	nd	0 08	0 11	nd	nd	nd	nd	nd
TiO_2	7 62	4.53	1 26	0.62	0.52	11.3	7.86	16.8	6.18	3.53	3.17	49 9	50.0	97 2	57 7
Al_2O_3	0.36	0.21	nd	nd	0.06	0.83	0.45	1.46	0.64	1.40	0.22	nd	nd	nd	0.15
V_2O_3	0.43	0.46	0.12	0.75	0.95	0.93	0.90	0 45	0.99	0 80	0.35	0.46	0.36	0.21	0.25
Fe_2O_3*	52 7	59.5	66 0	66.8	66.1	43.8	52.4	34 3	54.2	59.6	62.2	–	–	–	–
FeO*	33.5	33.1	27.6	30 2	30.7	36.5	35.7	42.4	35.0	33 1	30.8	21 7	12.4	0.11	0.89
MnO	4.46	2.31	4.64	1.50	0.60	4.98	3.08	4 01	1.37	1.49	3.09	25.1	34.5	nd	nd
MgO	nd	nd	nd	nd	nd	nd	nd	0.05	nd	0.08	nd	nd	nd	nd	0.67
CaO	0.03	nd	nd	0.03	0 21	nd	nd	nd	0.13	0.05	0.06	0.21	nd	nd	40.0
Nb_2O_5	0 07	0.06	nd	nd	nd	0.06	nd	na	nd	nd	nd	1.94	1.83	2 19	0 59
Sum	99.17	100.20	99.69	99.97	99.30	98.58	100.54	99.47	98.59	100.16	99.89	99.31	99 09	99.71	100.25
No. pts averaged	3	3	3	4	5	3	3	3	3	4	6	7	14	9	4

nd = not detected, na = not analyzed. Cr analyzed for but not detected except in magnetite from 83-32 (no. 6). Columns are as follows: 1, 2–Core and rim, respectively, of Type I magnetite partly included in K-feldspar, 3–Type II magnetite intergrown with biotite (Table 6, no. 1), intergrowth forms pseudomorph after clinopyroxenes, 4–Type III magnetite intergrown with ilmenite (this table, no 12) and aegirine (Table 3, no. 4); 5–Type IV magnetite intergrown with fluorite, rinkite, garnet, and aegirine; 6, 7–Core and rim, respectively, of Type I magnetite with embayed margins (sum of no. 6 includes 0.07 wt.% Cr_2O_3); 8–Core of most Ti-rich magnetite (Type I) analyzed from Magnet Cove syenites Rim of this grain is similar in composition to no. 6, this table. 9–Groundmass grain Overall range of TiO_2 is 3.23–7.75 wt.% and of MnO is 0.55–1.62 wt.%; 10–Rimmed by sphene (Table 7, no. 7); 11–Groundmass grain with a range of 1 30–5.32 wt.% TiO_2 and 1.75–4.93 wt % MnO, 12–Intergrown with magnetite (no 4, this table) and aegirine (Table 3, no. 4); 13–Intergrown with aegirine replacing aegirine-augite. Range of Nb_2O_5 is 0.67–4.38 wt.%, 14–Growing in vugs with lorenzenite. Range of Nb_2O_5 is 0.98–3.71 wt.%; 15–Marginally replaced by melanite garnet. *Fe^{3+} and Fe^{2+} calculated by assuming ideal stoichiometry of 3 cations per 4 anions for magnetite, all Fe as Fe^{2+} for ilmenite and perovskite.

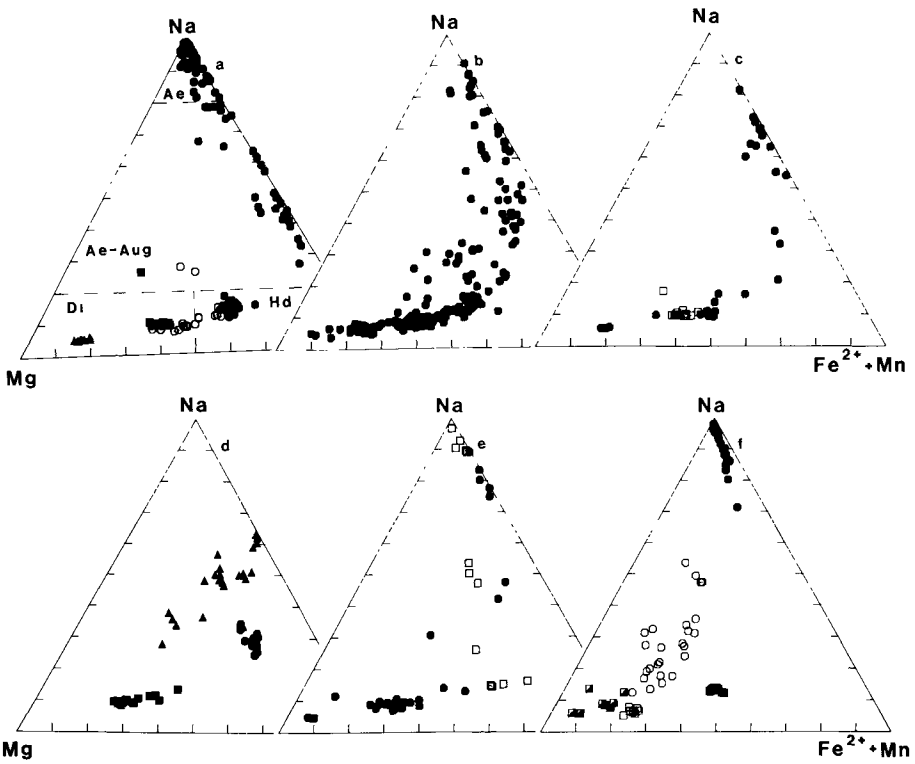

Fig. 8. Electron microprobe analyses of clinopyroxenes from syenites plotted in the system Na–Mg–(Fe^{2+} + Mn) (cations). (a) Diamond Jo nepheline syenite (filled hexagons) and pseudoleucite syenites 1-DJ11 (open hexagons), 83-32 (filled triangles) and 86-55B (filled squares); (b) garnet–nepheline syenites from Diamond Jo quarry; (c) garnet–nepheline syenites 85-55 (open squares) and 86-60 (filled hexagons); (d) sphene–nepheline syenite (filled squares) and miscellaneous nepheline syenites 86-64 (filled hexagons) and 85-17 (filled triangles); (e) alkali syenite 83-51 (open squares) and miscellaneous nepheline syenite 86-62B (filled hexagons); (f) miscellaneous nepheline syenites 84-20 (from garnet-rich nepheline syenite and sphene-rich reaction zone–open hexagons; from pegmatitic part–filled hexagons) and 85-14B (groundmass grains–filled squares; phenocrysts–open squares; anhedral grains intergrown with biotite within phenocrysts–half-filled squares). Clinopyroxene fields in (a): Di–diopside; Hd–hedenbergite; Ae-Aug–aegirine-augite; Ae–aegirine. Clinopyroxene nomenclature of Morimoto (1988).

ilar to spodiophyllite described from the Lovozero massif by Vlasov et al., 1966), accessory pyrophanite, barite and Zn-bearing sulfide. Laths of aegirine (Table 3, no. 3) form rosettes that are compositionally similar to aegirine that mantles the grains of aegirine-augite. Tabular, brown K-feldspar is replaced by natrolite and sodalite (Fig. 9). Sodalite rarely occurs in contact with the K-feldspar; natrolite typically forms between these two minerals.

Pseudoleucite syenite

Samples of pseudoleucite syenite, with different proportions of pseudoleucites to groundmass, grains sizes, modes and accessory minerals, were collected from three different localities (Fig. 1). The groundmass consists of laths of K-feldspar and smaller amounts of clinopyroxene, melanite garnet, biotite, nepheline, cancrinite, zeolite, calcite, magnetite and apatite. Rinkite, sphene and fluorite are found only in the groundmass of pseudoleucite syenite from Diamond Jo quarry; pyrite, calcite and magnetite are more abundant in sample 83-32 than in other samples. Samples with relatively abundant K-feldspar have a trachytoid texture, whereas relatively mafic samples have an intergranular texture.

Pseudoleucites, which are as much as 2.5 cm across, are composed of intergrown K-feldspar and nepheline or K-feldspar and fine-grained intergrowths of analcime and K-feldspar. Where nepheline is present, it is partly replaced by cancrinite and natrolite. Al-hydroxide and Al-rich clay are present in nepheline-free pseudoleucites and they may be alteration products of nepheline, cancrinite and/or

TABLE 5

Representative compositions of garnet from syenites

Sample	Diamond Jo neph. syenite		Garnet-nepheline syenite				Sph.-neph. sy.	Miscellaneous nepheline-syenites			
	2-100		83-31			3-157	85-15B	84-20		85-14B	86-64
	1	2	3	4	5	6	7	8	9	10	11
wt %											
SiO_2	32.0	33.2	30.9	33.2	32.5	33.4	34.9	30.2	33 8	35.3	33.1
TiO_2	7.51	4.72	9 47	5.56	7.09	2.25	2.94	11.7	6.30	2.36	5.06
ZrO_2	0 13	0.17	0.15	0 14	0.26	1.25	0 49	0.31	0.10	0.40	0.44
Al_2O_3	1.54	2.28	2.78	2.40	1.74	7.37	4.18	0.55	0.25	5 63	1.10
V_2O_3	0 72	0.63	na	na	na	0.61	0 22	0.55	0.39	0.44	0.29
Fe_2O_3*	23 2	24.9	21.7	24.8	23.7	18.4	22 3	20.5	24.0	20.6	26.6
FeO*	2.26	0.67	1.23	1.11	1.61	0	2.11	2.43	1.21	1.98	0.95
MnO	1.05	0.95	0.72	1.09	0.92	0.53	0.65	0.52	0.34	1.43	1.47
MgO	0.22	0.30	0.72	0.49	0.51	0.15	0.28	0.74	0.51	0.26	0.47
CaO	31.6	32.2	32.6	32 2	32.2	34.5	32.0	31.7	32 5	31.5	31.1
Na_2O	0.20	0.11	0.12	0.11	0.14	0.11	0 10	0.43	0.44	0.06	0.27
F	na	na	na	na	na	1.78	na	nd	nd	na	na
Sum	100.43	100.13	100.39	101 10	100 67	99.60**	100 17	99.63	99.84	99.96	100.85
Cations											
Si	2.698	2.784	2.586	2.761	2.720	2.705	2.897	2.569	2.844	2 910	2.780
Al	0.153	0.216	0.274	0.235	0.172	0 123	0.103	0.055	0.025	0.090	0 109
Fe^{3+}	0.149	0	0 140	0.004	0.108	0	0	0.376	0 131	0	0.111
	3.000	3.000	3.000	3.000	3.000	3.000#	3.000	3.000	3.000	3.000	3.000
Al	0	0.009	0	0	0	0.581	0 305	0	0	0.458	0
Ti	0.476	0.298	0.596	0.348	0.446	0.137	0.183	0.750	0.399	0.147	0.319
Zr	0.006	0.008	0 007	0.007	0.012	0.057	0.023	0.015	0.005	0.019	0.021
V	0.049	0.042	–	–	–	0.040	0 015	0.038	0.026	0.029	0 020
Fe^{3+}	1.322	1 571	1.227	1 547	1.386	1.124	1.390	0.933	1.393	1.281	1.566
Fe^{2+}	0.119	0.035	0.080	0 041	0.092	0	0.049	0.170	0.085	0.034	0.059
Mg	0.028	0 037	0.090	0.057	0.064	0.018	0.035	0.094	0.064	0.032	0 015
Mn	0	0	0	0	0	0 036	0	0	0 024	0	0
	2.000	2.000	2.000	2.000	2 000	1.993	2.000	2.000	1.996	2.000	2.000
Fe^{2+}	0.040	0.012	0.006	0.036	0.021	0	0.097	0.003	0	0.102	0.052
Mn	0 075	0.067	0.051	0.077	0.065	0	0.046	0.037	0	0.100	0.104
Ca	2.852	2.902	2.923	2.870	2.892	2.992	2 841	2.889	2.931	2.787	2.799
Na	0.033	0.018	0.019	0.018	0.023	0 017	0.016	0.071	0.072	0.010	0.044
	3.000	2.999	2.999	3.001	3 001	3.009	3.000	3.000	3.003	2.999	2.999
No pts. averaged	3	3	5	6	3	3	5	6	3	5	6

nd = not detected; na = not analyzed. Columns are as follows: 1, 2–Core and rim, respectively, of zoned euhedral grain; 3 to 5–Complexely zoned grain: euhedral dark-red core (no. 3) is discontinuously zoned to lighter-red melanite (no 4) that contains a dark-red zone (no. 5); 6–Colorless, slightly birefringent overgrowth of fluoro-hydrograndite garnet; 7–Anhedral inclusions within andesine; 8, 9–From nepheline syenite and reaction zone, respectively; 10–Anhedral grains in groundmass, 11–Sieve-textured grains containing numerous inclusions of K-feldspar. *Fe^{3+} and Fe^{2+} calculated by assuming ideal stoichiometry of 8 cations per 12 oxygens. **Oxide sum adjusted for oxygen equivalent of F. #Tetrahedral site sum includes OH/4 = 0.059 and F/4 = 0.114; OH is calculated by assuming that the difference between 100% and the oxide sum is equal to the water content; see Flohr and Ross (1989) for detailed explanation of calculation of mineral formulae of F-bearing garnets.

TABLE 6

Representative compositions of micas from syenites

Sample	Diamond Jo neph. syenite	Pseudoleucite syenite	Garn.–neph syenite	Miscell. neph. sy.
	2-100	1-DJ11	86-60	85-14B
	1	2	3	4
wt.%				
SiO_2	34.3	32 9	38 4	41.2
TiO_2	1.05	2.13	1.77	0.97
Al_2O_3	11.8	6.69	12.8	12.5
V_2O_3	0 07	0 19	0.15	0.06
FeO	26 1	41 3	15 8	9.23
MnO	9 30	2.45	0 91	0.53
MgO	3.67	1.36	16.0	21 7
CaO	0.07	0.04	0.03	0.04
BaO	nd	0.03	0.14	0.16
Na_2O	0.15	0.09	0.13	0.40
K_2O	8.87	8 27	9.82	9.44
F	0.14	nd	1.53	3 85
Sum	95 52	95.45	97.48	100.08
-F≡oxy	0.06		0.64	1 62
Sum	95 46		96.84	98.46
Cations				
Si	2.854	2.894	2.880	2.959
Al	1.146	0.693	1.120	1.041
	4.000	3.587	4.000	4.000
Al	0.010	0	0.100	0.019
Ti	0.066	0 141	0.012	0 052
V	0.005	0.013	0.009	0.004
Fe	1.819	3.035	0 991	0.554
Mn	0 656	0 182	0.058	0.032
Mg	0.455	0.178	1.790	2.325
	3.011	3.549	2 960	2.986
Ca	0.006	0.004	0.002	0 003
Ba	–	0.001	0.004	0 005
K	0.942	0.927	0.941	0.865
Na	0.024	0 015	0.019	0.056
	0.972	0.947	0.966	0.929
F*	0.037	–	0 363	0.874
No pts. averaged	3	3	5	4

Cations calculated to 11 oxygen equivalents assuming all Fe as Fe^{2+}, Cl analyzed for, but not detected; nd = not detected. Columns are as follows. 1–Biotite intergrown with magnetite (Table 4, no. 3). The intergrowth forms a pseudomorph after pyroxene; 2–Fe-rich biotite that replaces pyroxene, 3–Biotite rimming pyroxene, 4–Phlogopite intergrown with anhedral grains of Mg-rich diopside within a diopside phenocryst (Table 3, no. 14). *F per formula unit calculated by assuming (OH + F) = 2

natrolite. Sodalite is a rare accessory phase in some pseudoleucites.

K-feldspar (Table 2, no. 4; Fig. 7b) within pseudoleucites is nearly Ba-free whereas laths of K-feldspar in the groundmass contain more Ba (Fig. 7c). These laths have zoning trends similar to those observed in K-feldspar from Diamond Jo nepheline syenite and are commonly rimmed by turbid, Ba-poor K-feldspar.

The composition of nepheline (Table 8) in pseudoleucite syenites lies within the Morozewicz–Buerger convergence field. Nepheline contains 0.4–1.2 wt.% FeO.

Pyroxene (Fig. 8a) compositions range from aluminian diopsides to low-Na aegirine-augites. All pyroxenes are normally zoned with Mg, Al and Ti decreasing from core to rim; overall zoning trends are similar to those found in pyroxenes from garnet–nepheline syenite described below. Pyroxenes from pseudoleucite syenite are not as Fe-rich or Na-rich as those from Diamond Jo nepheline syenite. Pyroxene is partly to completely replaced by biotite (Table 6, no. 2) or biotite plus magnetite.

Sphene, rinkite (Table 7, no. 4, 10), melanite and magnetite are accessory minerals. Melanite is zoned, with decreasing TiO_2 ($\sim$10–6 wt.%) from core to rim, and is rimmed by a colourless, slightly birefringent garnet. Primary Type I magnetite (Table 4, no. 6, 7) forms relatively coarse grains, whereas Type II and Type III magnetite occur in replacement assemblages. Type II magnetite is intergrown with biotite and has, on average, lower MnO concentrations (0.31–2.16 wt.%) than Type II magnetite from Diamond Jo nepheline syenite. Type III magnetite is intergrown with Fe-sulfide and an Mn-rich, Nb-poor ilmenite (21.4 wt.% MnO, 0.14 wt.% Nb_2O_5).

Garnet-nepheline syenite

Several distinct stages of crystallization and replacement are observed in garnet–nepheline syenite. Apatite and Ti-bearing magnetite began to crystallize first and were followed by perovskite and diopside. Aegirine-augite and nepheline crystallized together and were followed by wollastonite, melanite and sphene, the latter replacing perovskite. Ba-bearing K-feldspar and then a turbid Ba-poor K-feldspar crystallized. (This feldspar paragenesis is similar to that seen in feldspars in Diamond Jo nepheline syenite.) Fe-rich biotite re-

TABLE 7

Representative compositions of accessory minerals from syenites

Sample	Diamond Jo nepheline syenite		Miscell. neph. sy.	Pseudol. syenite	Garn.–neph. sy	Sph.–neph sy	Miscellaneous nepheline syenites			Pseudol. syenite	Garn.–neph. sy
	Wollastonite	Spodiophyllite	Pectolite	Sphene						Rinkite	
	2-DJ7	2-DJ7	84-20	1-DJ11	1-71C	85-15B	84-20	85-14B		1-DJ11	1-71C
	1	2	3	4	5	6	7	8	9	10	11
wt.%											
SiO_2	50.1	50.6	52.3	30.4	30.6	30.2	30.1	30.8	30.2	32.9	33.2
TiO_2	0.05	1.54	0.11	31.9	33.1	33.9	35.5	31.2	36.1	8.98	9.70
ZrO_2	na	na	0.19	0.66	1.39	0.49	0.96	0.62	0.31	0.58	0.93
Al_2O_3	nd	5.60	0.11	0.94	0.79	1.84	0.43	3.17	1.13	nd	nd
V_2O_3	na	nd	nd	0.39	0.33	0.39	0.47	0.47	0.48	0.08	0.11
FeO	1.48	2.80	0.09	2.37	1.47	1.47	1.65	2.34	1.12	0.37	0.22
MnO	1.38	1.65	3.60	nd	nd	0.06	nd	0.08	nd	0.37	0.51
MgO	0.15	18.3	0.34	0.17	0.15	0.19	0.18	0.24	0.18	0.23	0.21
CaO	45.5	nd	29.5	27.3	27.4	27.5	28.1	27.9	28.4	41.5	41.6
Na_2O	nd	0.12	8.99	0.36	0.31	0.07	0.10	0.07	0.04	5.27	5.12
K_2O	nd	10.7	nd	na	na	na	na	na	na	na	na
Nb_2O_5	na	na	na	2.63	2.33	0.52	0.31	0.62	0.24	1.63	0.78
La_2O_3	na	na	na	0.26	0.06	0.20	0.07	0.09	nd	0.73	0.14
Ce_2O_3	na	na	na	0.32	0.26	0.43	0.16	0.29	0.23	0.71	0.16
F	na	na	na	0.42	0.61	1.01	0.30	1.96	0.59	8.81	10 6
Sum	98.66	91.31	95.23	98.12	98.80	98.27	98.23	99.85	99.02	102.16	103.28
-F≡oxy				0.18	0.26	0.42	0.13	0.82	0.25	3.71	4.47
Sum				97.94	98.54	97.85	98.10	99.03	98.77	98.45	98.81
No. pts. averaged	3	3	3	4	3	6	3	4	6	4	7

nd = not detected; na = not analyzed. Columns are as follows: 1–Inclusions in Ba-bearing K-feldspar; 2–Mineral tentatively identified as spodiophyllite that forms hexagonal and tabular brown grains in groundmass of natrolite, sodalite, and aegirine; 3–From sphene-rich reaction zone; 4, 5–Intergrown with rinkite (this table, no. 10 and 11, respectively); 6–Euhedral grain in groundmass; 7–From sphene-rich reaction zone; 8, 9–Rims magnetite (Table 4, no. 10) and forms euhedral grains in groundmass, respectively; 10, 11–Intergrown with sphene (this table, no. 4 and 5, respectively). Rinkite in 1-71C forms clusters of radiating laths.

places pyroxene. Rinkite, sphene, fluorite, calcite and colourless, birefringent garnet were the last minerals to crystallize. Rinkite and fluorite are common in garnet–nepheline syenites from Diamond Jo quarry but are rare in syenites from other localities.

Pyroxene from garnet–nepheline syenite shows a complex crystallization history. Relic cores of pale-pink subsilicic diopside (Table 3, no. 5) are continuously zoned with both Al and Ti increasing as $Mg/(Mg+Fe^{2+}+Fe^{3+}+Mn)$ decreases. In other grains, cores appear optically mottled, with relatively Al-, Ti- and Fe-rich pink diopside replacing more Mg-rich and Al- and Ti-poor, light-green diopside. Still other grains have cores of diopside (Table 3, no. 6) that are more Fe-rich than the pink diopside. All three types of cores have resorbed margins and are rimmed by aegirine-augite (Table 3, no. 7), which is zoned with Al, Ti and Mg decreasing outward to the rim. Laths of normally zoned aegirine-augite (Table 3, no. 8) are common. Although individual grains are discontinuously zoned, as described above, the overall trend is one of increasing Na and Fe as Mg decreases (Fig. 8b, c). Pyroxene laths within mafic segregations range in composition from Al- and Ti-bearing diopside to aegirine-augite;

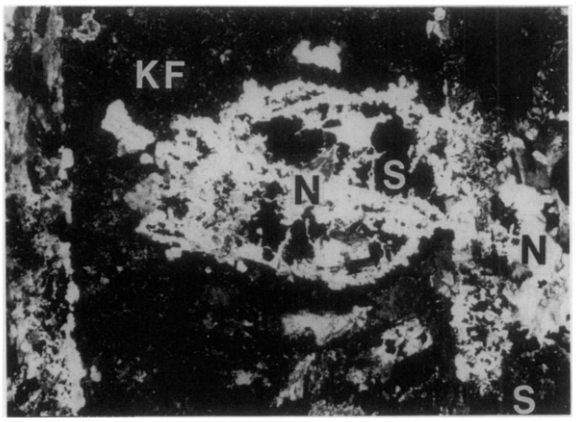

Fig. 9. Part of pegmatitic segregation within Diamond Jo nepheline syenite sample 2-DJ7. Turbid K-feldspar (*KF*) is partially replaced by sodalite (*S*) and natrolite (*N*) that invade the grain from the surrounding groundmass. Transmitted light, crossed nicols. Field of view is 5 mm across.

compositionally, these laths are within the range of pyroxenes that occur outside the segregations.

Zoning in K-feldspar (Fig. 10) is further evidence for a complex crystallization history. Crystallization of Ba-free K-feldspar both before and after Ba-rich K-feldspar is indicated by the zoning observed in one grain (Fig. 10a). A second complex grain shown in Fig. 10b and 10c consists of a perthitic core, in which the more abundant feldspar contains 18.2–19.9 wt.% BaO and the less abundant feldspar 9.32–9.66 wt.% BaO (Table 2, no. 5, 6). The core is rimmed by non-perthitic feldspar containing 8.49–9.21 wt.% BaO.

K-feldspar (Fig. 7d), which is compositionally and texturally like the Ba-rich mantle of the grain shown in Fig. 10a, is more common than such complexly zoned grains. The common grains poikilitically include euhedral to subhedral grains of diopside, melanite, nepheline and rare wollastonite and are rimmed by brown, turbid Ba-poor K-feldspar. Anhedral grains of K-feldspar within mafic segregations are compositionally similar to groundmass grains.

Nepheline is very similar in composition to that found in pseudoleucite syenite, with a range of about 0.5 to 1.0 wt.% FeO.

Melanite, containing 12.4 to 4.15 wt.% TiO_2, has a wider range of compositions than melanite from either Diamond Jo nepheline syenite or pseudoleucite syenite. Complex, oscillatory zoning is observed (Table 5, no. 3 to 5; see also fig. 3 of Flohr and Ross, 1985). Melanite within the mafic-rich segregations is compositionally like melanite in the surrounding groundmass. Fluorine-bearing garnet (Table 5, no. 6) is found as overgrowths on melanite, as fracture fillings, and in replacement intergrowths as observed in Diamond Jo nepheline syenite.

Accessory minerals include sphene, rinkite (Table 7, no. 5, 11, respectively), perovskite (Table 4, no. 15), magnetite and biotite (Table 6, no. 3), with an Mg/(Mg+Fe+Mn) range of 0.234 to 0.657. Primary Type I magnetite (Table 4, no. 8) is more Ti-rich than Type II magnetite which forms anhed-

TABLE 8

Representative compositions of nepheline from syenites

Sample	Pseudoleucite syenite	Sph -neph. syenite	Miscellaneous nepheline syenites		
	1-DJ11	85-15B	84-20	85-14B	86-64
wt.%					
SiO_2	41 9	44.0	41.7	44.1	44.1
Al_2O_3	34.5	34 1	34.5	33.9	32.5
FeO	1.13	0.28	1.71	0.49	0 57
MgO	nd	nd	nd	nd	nd
CaO	nd	0.75	0.04	1.75	0.16
BaO	nd	nd	na	na	nd
Na_2O	15 3	15.6	15.7	14.5	16.1
K_2O	7 69	5.74	7 14	4.51	6.42
Sum	100.52	100.47	100.79	99.25	99.85
Cations					
Si	8 106	8.382	8.054	8 432	8.502
Al	7.855	7.645	7.852	7.635	7.386
	15.961	16.027	15.906	16.067	15.888
Fe	0.183	0.045	0.276	0.078	0.092
Mg	0	0	0	0	0
Ca	0	0.153	0.008	0 358	0.033
Ba	0	0	0	0	0
Na	5.738	5.745	5.886	5.367	5.999
K	1.895	1.393	1.760	1 099	1.578
	7.816	7.336	7.930	6.902	7.702
Molecular proportions					
FeNe	2.7	0.7	4.0	1.2	1.4
An	0	3.7	0.2	8.9	0.8
Ks	26.1	19.3	23.9	15.5	21.7
Ne	68.7	71.5	68.4	68.1	70.8
Qz	2.5	4.8	3.5	6.2	5.3

Cations calculated per 32 oxygens, nd=not detected; na=not analyzed; FeNe=hypothetical Fe-nepheline; An=anorthite; Ks=kalsilite; Ne=nepheline; Qz=quartz. Endmembers calculated assuming all Fe is ferric Each analysis is a 3-point average.

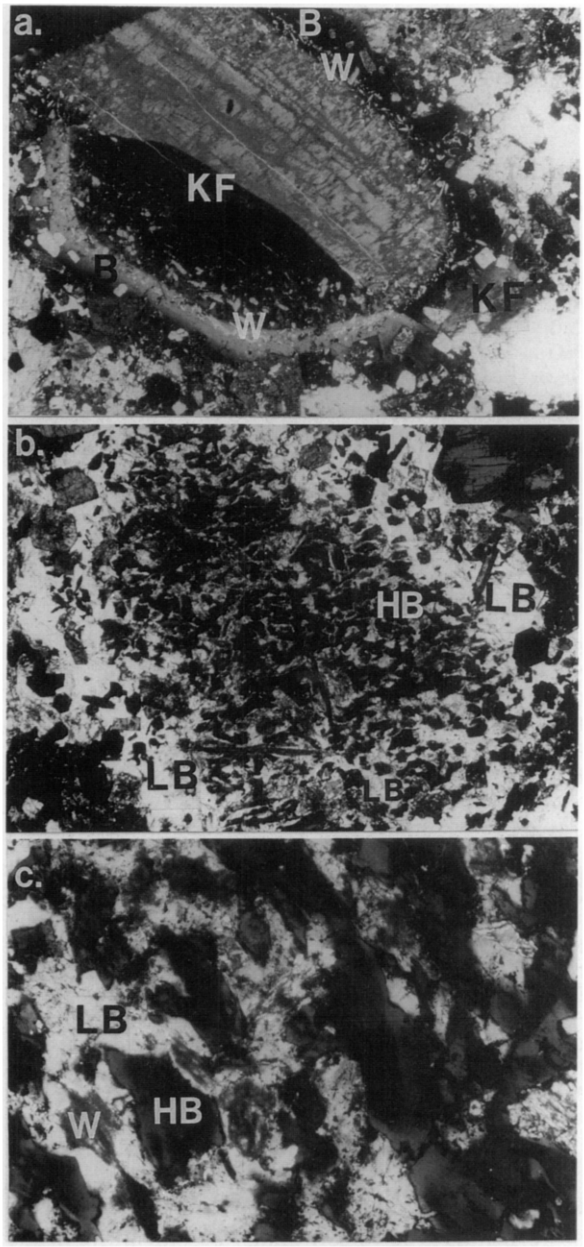

ral grains intergrown with sphene replacing perovskite.

Sphene–nepheline syenite

Sphene–nepheline syenite is a medium-grained rock with a hypidiomorphic texture. Euhedral to subhedral amphibole, sphene (Table 7, no. 6) and clinopyroxene (Fig. 8d) are partly enclosed by laths of andesine, perthitic Ba-poor alkali feldspar (Fig. 7e) and nepheline (Table 8). Amphibole forms rare phenocrysts and contains inclusions of sphene. Plagioclase is replaced at its margins by microperthitic sodic K-feldspar (Table 2, no. 7, 8). Anhedral sodalite, magnetite (Table 4, no. 9) and secondary analcime are accessory phases. Nepheline is locally altered to zeolite. Minor amounts of natrolite, presumably the result of alteration and blebs of melanite (Table 5, no. 7) occur within plagioclase.

Mafic segregations consist of euhedral to subhedral amphibole, with accessory sphene and magnetite and only minor clinopyroxene and interstitial sodalite, feldspar (presumably cryptoperthitic, with a wide range of Na/K) and nepheline. These segregations have rounded to scalloped margins.

Amphibole grains are discontinuously zoned. Grains in the mafic segregations have cores of pargasite (Table 9, no. 1) and rims of ferroan pargasite. Phenocrysts have cores of pargasite and rims of hastingsite (Table 9, no. 2, 3). The cores, which are continuously zoned with decreasing Ti and Mg towards the rim, are similar in composition to the rims of the pargasites that occur in mafic segregations. Hastingsite also rims pyroxene, which is continuously zoned from diopside to hedenbergite (Table 3, no. 9, 10).

Alkali syenite

Alkali syenite 83-51 is vuggy and composed of

Fig. 10. (a) Twinned grain of Ba-free K-feldspar (*KF*) mantled by Ba-rich K-feldspar (B; 4.57–8.24 wt.% BaO). A zone (*W*) containing abundant inclusions of wollastonite lies within both KF and B feldspars. B contains abundant inclusions of melanite (black), pyroxene (various shades of gray), and nepheline (white-gray with rectangular cross-section). B is partly mantled by K-feldspar (KF′) containing very low Ba. Garnet–nepheline syenite 3-157. Transmitted light, crossed nicols. Field of view is ~1 cm across. (b) Grain consisting of perthitic intergrowth of two Ba-rich feldspars. Feldspar with relatively high Ba (*HB*) is found only in the interior of the grain and is near extinction (dark). Feldspar with lower Ba (*LB*) is found in the interior of the grain (light areas surrounding *HB*) and also mantles the intergrowth. Grains of melanite (black), pyroxene, and nepheline are included in the mantle. Partly altered grains of wollastonite are found in the interior. Garnet–nepheline syenite A-DJ10. Transmitted light, crossed nicols. Field of view is 9 mm across. (c) Close-up of lower right section of grain shown in (b), showing perthitic intergrowth of low-Ba (*LB*) and high-Ba (*HB*) feldspar. *W*=wollastonite. Transmitted light, crossed nicols. Field of view is 2 mm across.

about 82 vol.% K-feldspar (Fig. 7f) and 7 vol.% aegirine-augite plus aegirine (T. Armbrustmacher, written commun., 1985). Amphibole, apatite and primary Type I magnetite are accessory minerals. Rare patches of clear K-feldspar, containing as much as 3.21 wt.% BaO, are mantled by turbid, brown, microperthitic, Ba-poor K-feldspar that is, in turn, rimmed by albite (Table 2, no. 9). Aegirine-augite (Fig. 8e) is discontinuously zoned from Na-poor cores to Na-rich rims. Overgrowths of Ti-rich aegirine occur on some grains. Richterite (Table 9, no. 5) is rimmed by sodic pyroxene or arfvedsonite (Table 9, no. 6), containing excess alkali in the A-site. The discontinuous zoning of richterite to arfvedsonite is analogous to the zoning trends found in pyroxenes. Anatase (Table 4, no. 14), lorenzenite, aegirine and K-feldspar (Fig. 7f) occur in vugs.

Miscellaneous nepheline syenites

Several nepheline syenites that differ in one or more respects from the rocks described in the preceding sections are briefly described below.

Nepheline syenite 85-17 is texturally and modally similar to the most felsic of the garnet–nepheline syenites. Pyroxene (Fig. 8d) is zoned from relatively Mg-rich (Table 3, no. 11) to Fe-rich aegirine-augite and defines a crystallization trend quite different from those of the syenites already described (Fig. 8a–c). K-feldspar (Fig. 7g) contains moderate amounts of Ba. Other minerals have compositions that fall within the ranges found in Diamond Jo nepheline syenite, but 85-17 lacks rinkite and contains little fluorite. Sphene is common and replaces melanite, rims magnetite and forms euhedral grains associated with cancrinite.

Nepheline syenite 84-20 is composed of three modally and texturally distinct lithologies. The most abundant lithology is an equigranular nepheline syenite containing pyroxene (Fig. 8f; Table 3, no. 12), melanite (Table 5, no. 8), K-feldspar (Fig. 7h), relatively K-rich nepheline (Table 8) and sphene that is modally subordinate to melanite. The second lithology is a pegmatite containing natrolite and zoned euhedral to subhedral aegirine and aegirine-augite (Fig. 8f). Minute laths of aegirine (Table 3, no. 13), altered sphene rimmed by pectolite (Table 7, no. 3) and aegirine-augite form aggregates within masses of natrolite. A reaction zone between nepheline syenite and pegmatite forms the third lithology. It consists of pyroxene (which is compositionally like that in the nepheline syenite), thomsonite, nepheline (which is partly replaced by a zeolite that is similar in composition to gonnardite), sphene and melanite. Sphene (Table 7, no. 7) is more abundant and garnet (Table 5, no. 9) is less abundant in the reaction zone than in the nepheline syenite.

Nepheline syenite samples 85-14B and 86-56A (Table 1) are of a faintly banded, equigranular rock from the undivided trachyte–phonolite unit (Fig. 1). These samples are coarser grained than the phonolite samples described by Erickson and Blade (1963). The nepheline syenite consists of anhedral grains of nepheline (Table 8), K-feldspar (Fig. 7h), clinopyroxene and accessory garnet (Table 5, no. 10), magnetite (Table 4, no. 10), sphene (Table 7, no. 8, 9), pyrrhotite, phlogopite (Table 6, no. 4) and apatite. Phenocrysts of diopside (Table 3, no. 14) contain abundant inclusions of anhedral sphene and are marginally replaced by magnesian hastingsite (Table 9, no. 4), which is in turn rimmed by hedenbergite, compositionally equivalent to the groundmass pyroxene (Table 3, no. 15). The crystallization of amphibole produced a discontinuity between pyroxene phenocryst and groundmass compositions (Fig. 8f).

Nepheline syenite 86-62B comes from an outcrop that is cut by a fine-grained biotite-rich melteigite–ijolite dike (sample 86-62A). This outcrop was found by Mike Howard (Arkansas Geological Commission) within the trachyte–phonolite unit (Erickson and Blade, 1963). This syenite is texturally and mineralogically similar to garnet–nepheline syenite, but certain trace-element abundances (Table 1), e.g., Th, U and Pb, set it apart from it. The syenite is severely altered, such that most of the nepheline is replaced by cancrinite and zeolite. Relic, Ba-bearing K-feldspar is mantled by Ba-poor feldspar (Fig. 7h). Pyroxene (Fig. 8e) is discontinuously zoned from cores of diopside to rims of aegirine-augite. Ti-rich aegirine-augite and aegirine form rare spherulites.

Nepheline syenite 86-64 consists of sieve-textured melanite (Table 5, no. 11), aegirine-augite (Table 3, no. 16; Fig. 8d) and magnetite. These minerals form anhedral grains interstitial to and intergrown with subhedral to anhedral Na-rich feldspar, K-feldspar (Fig. 7i) and nepheline (Table 8). Sodalite, sphene, Fe-rich biotite and cancrinite are minor phases. The rock has a banded appearance

TABLE 9

Representative compositions of amphibole from syenites

Sample	Sphene-nepheline syenite			Misc. neph sy	Alkali syenite	
	85-15B			85-14B	83-51	
	1	2	3	4	5	6
wt.%						
SiO_2	39 7	38.8	38.6	40.9	53.1	55.1
TiO_2	4.35	3.28	1.55	1.21	0 57	0.32
Al_2O_3	13.9	13.2	12 6	11 7	0.15	0.12
V_2O_3	0.08	0.11	0 10	0.05	0.04	0.03
Fe_2O_3*	0.52	2.10	4 79	4.39	2.75	7 88
FeO*	9.30	16.6	19 6	13.3	16.2	3.37
MnO	0.22	0.55	0.64	1 10	1.01	5.13
MgO	14.0	8.78	6.10	10 6	11.4	13.5
CaO	12.1	11.2	11 0	11 5	5.05	1.40
BaO	0.14	0.06	nd	nd	nd	nd
Na_2O	2.56	2.55	2.58	2.58	6 59	9.27
K_2O	1.88	2.00	1.91	1 95	1.81	1.98
F	1.02	0.67	0.63	1.83	2.92	3 21
Sum	99.77	99.90	100.10	100.10	101.59	101.31
-F≡oxy	0.43	0.28	0 27	0.77	1 23	1.35
Sum	99 34	99.62	99 83	100.34	100.36	99.96
Cations						
Si	5.822	5.885	5.960	6.142	7.887	7 980
Al	2.178	2.115	2.040	1.858	0.026	0.020
	8.000	8.000	8.000	8.000	7.913	2.000
Al	0.230	0.251	0 260	0.207	0 000	0.000
Ti	0.480	0.374	0.180	0.137	0.064	0.035
V	0.009	0.013	0 012	0.006	0.005	0.003
Fe^{3+}*	0.057	0.240	0.557	0.495	0.307	0.857
Fe^{2+}*	1.142	2.103	2.534	1 664	2.016	0.408
Mn	0.025	0.033	0.052	0.112	0.087	0.629
Mg	3.057	1.986	1 405	2.379	2.521	2.909
	5.000	5 000	5.000	5.000	5.000	4.841
Mn	0.002	0.038	0.032	0.028	0.040	0.000
Na	0.090	0 141	0.150	0.122	1.156	1.783
Ca	1.908	1.821	1.818	1.850	0 804	0.217
	2.000	2.000	2.000	2 000	2.000	2.000
Na	0.639	0.609	0.623	0.628	0.742	0.817
K	0.352	0.387	0.377	0 373	0.343	0.365
Ba	0.008	0.004	0.001	0.000	0.000	0.002
	0.999	1.000	1.001	1 001	1.085	1.184
F**	0.474	0 322	0.308	0.868	1.372	1.469
No. pts. averaged	3	5	4	4	4	4

Cr and Cl analyzed, but not detected. Columns are as follows: 1–Core of euhedral pargasite in mafic segregation; rim is similar to core of phenocrysts in surrounding groundmass (no. 2, this table); 2, 3–Core of ferroan pargasite and rim of magnesian hastingsite, respectively, of phenocryst, 4–Overgrowth of magnesian hastingsite on diopside phenocrysts (Table 4, no. 14); 5–Grain of richterite partly replaced by aegirine, 6–Euhedral magnesio-arfvedsonite in vug. *Fe^{2+} and Fe^{3+} calculated assuming stoichiometry of 16 cations per 23 anions for no. 1 to 5 and on the basis of 8 (Si+Al) for no 6. **F anions per formula unit calculated assuming (F+OH)=2.000.

defined by the abundance of garnet and a slight change in grain size.

Discussion

Relationship between garnet–nepheline syenite and pseudoleucite syenite

The K, Rb, Sr and Ba trends (Fig. 2g; Figs. 4a, b, c) defined by samples of pseudoleucite syenite and garnet–nepheline syenite are consistent with the two syenite groups having the same parent magma. Pseudoleucite syenites represent leucite cumulates and garnet–nepheline syenites crystallized from the residual magma. We propose the following model. Leucite, the presumed precursor of the pseudoleucites, was an early-crystallizing phase and removed Rb and Cs, but not Sr or Ba, from the melt. [During crystallization of leucite, large cations such as Cs^+ (Deer et al., 1963) and Rb^+ would readily enter the leucite structure. Rb^+ and Cs^+ would substitute for K^+, whereas Ba^{2+} and Sr^{2+} would be excluded and would concentrate in the residual magma. To maintain charge balance, the substitution of Ba or Sr for K would require a coupled substitution of Al for Si, or addition of a vacancy; apparently this type of substitution is limited in leucite (Deer et al., 1963)]. Leucite, being less dense than its relatively dense parent magma, began to float within the magma chamber and was removed from reaction with its residual magma. Subsequent crystallization of the leucite-bearing magma at relatively high levels of the chamber produced pseudoleucite syenite. In this model, because leucite is physically removed from the parent magma and cannot react with it (and be resorbed), the residual magma is enriched in Ba and Sr and depleted in K and Rb relative to the parent magma. Garnet–nepheline syenite crystallized from the residual magma and defines differentiation trends offset to lower K and Rb and higher Ba and Sr relative to the trends defined by pseudoleucite syenite.

The similarity in textures, mineralogy and mineral compositions found in garnet–nepheline syenite and the groundmass of pseudoleucite syenite is further evidence that pseudoleucite syenite and garnet–nepheline syenite are genetically related. Feldspar compositions overlap (Fig. 7c, d). Pyroxene compositions are also similar. The range of pyroxene compositions from the most mafic garnet–nepheline syenite (86-55; Fig. 8c) is nearly identical to the range of pyroxene compositions from the groundmass of the pseudoleucite syenite (86-55B; Fig. 8a) that is in contact with 86-55.

Evidence for multiple syenite magmas

At least four distinct parental syenite magmas are identified on the basis of the data obtained in this study. Garnet–nepheline syenite and pseudoleucite syenite share a common parent, as discussed above. Diamond Jo nepheline syenite, with lower Rb/Sr and Nb/Ta and higher Th/U and Zr/Hf than garnet–nepheline syenite (except for Nb/Ta in 86-55; Table 1) crystallized from a different magma. Sphene–nepheline syenite and alkali syenite are distinct from each other and the syenites of the other groups (Figs. 2, 4) and so represent two additional syenite magmas. The variety of pyroxene crystallization trends (Figs. 8, 11) and ranges of feldspar compositions (Fig. 7) reflect differences among the syenite magmas. How and if the miscellaneous nepheline syenites are related to each other or the other syenites is not clear at this time and each of these nepheline syenites may have been derived from a separate parent magma.

Syenites from Magnet Cove share several characteristics, despite the differences noted above. The very low $Mg/(Mg+Fe^2[T])$ (<0.2) of all the syenites analyzed in this study indicates that they were derived from magmas that underwent extensive fractionation. Very low abundances of Sc and Cr in all syenites indicate pyroxene fractionation and low abundances of Co indicate oxide fractionation (e.g., Rankama and Sahama, 1950; Currie et al., 1986).

Metasomatism

Pegmatitic segregations containing abundant sodalite, natrolite and aegirine crystallized from the Cl-, Na- and H_2O-rich residual magma of the Diamond Jo nepheline syenite. Crystallization of the syenite had progressed to the stage where pockets of the Cl-rich and, presumably, vapour-rich magma were trapped and were not able to coalesce to form larger segregations. The Na- and Cl-rich residuum reacted with primary minerals and as a result K-feldspar was replaced by natrolite and sodalite and

aegirine-augite by aegirine. Barite and spodiophyllite formed at this time. These replacement processes may be termed autometasomatism, as there is no evidence for an external source for the metasomatizing fluids.

Sodalite is not found in assemblages in Diamond Jo nepheline syenite that contain F-bearing minerals, suggesting that F and Cl were concentrated in different fractions of the magma during crystallization. Koster van Groos and Wyllie (1968, 1969) investigated the phase relationships in the systems $NaAlSi_3O_8$–H_2O–NaCl and $NaAlSi_3O_8$–H_2O–NaF. They found that chlorine (NaCl) was preferentially partitioned into the vapor phase, whereas fluorine (NaF) remained in the liquid phase. We suggest that the sodalite-bearing, Cl-rich pegmatitic segregations formed from the vapor-rich residual fraction of the magma and that F was concentrated in the liquid fraction that reacted with early-crystallized phases and formed the fluorite- and rinkite-bearing replacement assemblages described above. Contrary to the behavior of Cl in hydrous systems described by Koster van Groos and Wyllie (1968, 1969), Kogarko (1987) concluded that in dry agpaitic magmas Cl was concentrated in the liquid phase. The presence of natrolite, rather than an anhydrous sodic phase such as albite, and spodiophyllite indicates that the residuum of the nepheline syenite magma was hydrous.

The enrichment of Mn in Type II magnetite, ilmenite (Table 4, no. 3, 12, 13), and biotite (Table 6, no. 1–3) that formed late in the crystallization sequence reflects redistribution of Mn during late-stage metasomatism. Mn is concentrated in primary Type I magnetite (Table 4, no. 1, 2, 6–8) and to a lesser degree in primary pyroxenes and garnets. Reactions between these primary minerals and residual fluids released Mn into the fluid phase, making it available for incorporation into late-crystallizing phases. An analogous base-metal exchange process was documented by Ilton and Eugster (1989), who found that Mn (as well as Zn, Cu and Cd) was strongly fractionated into the fluid relative to Fe when magnetite reacted with chloride-rich hydrothermal fluid. They concluded that this process would result in significant concentrations of the minor elements in the fluid and considered applications to base-metal mineralization in skarn deposits.

The behaviour of Ti, V and Zr is similar to that of Mn described above. Ti is concentrated in perovskite, Type I magnetite, diopside and melanite. Zoning trends demonstrate that Ti is concentrated in the cores of these primary minerals relative to the rims. Type I magnetite also contains minor V and melanite contains both V and Zr. When late-crystallizing phases are considered, the following observations were made: aegirine (Table 3, no. 4), sphene, rinkite (Table 7) and ilmenite (Table 4, no. 12, 13) contain significant Ti; fluoro-hydrograndite (Table 5, no. 6), sphene and Type III and IV magnetites (Table 4, no. 4, 5) contain significant V; and fluoro-hydrograndite and rinkite contain significant Zr. Cl and F, which act as mineralizers in volatile-rich alkaline rocks (e.g., Kogarko, 1974), may have been responsible for the local mobilization of metal such as Ti, V, Zr and Mn during the late stages of magmatism at Magnet Cove.

Fluorite and rinkite are common in pseudoleucite syenite and garnet–nepheline syenite from Diamond Jo quarry, but are not common in relatively F-poor pseudoleucite syenite and garnet–nepheline syenite (84-25, 85-55, 86-55B, 86-60; Table 1) collected from other localities, indicating a heterogeneous distribution of F in the parent magma. Alternatively, garnet–nepheline syenite and pseudoleucite syenite from Diamond Jo quarry may have been metasomatized by F-bearing fluid from the Diamond Jo nepheline syenite magma. A chill zone between Diamond Jo nepheline syenite, which intruded after the pseudoleucite syenite (Erickson and Blade, 1963) and pseudoleucite syenite is not evident, indicating that the two syenites were in or close to thermal equilibrium and that volatile or fluid exchange may have been possible. However, whole-rock F content and abundance of F-rich minerals in the syenites adjacent to the Diamond Jo nepheline syenite are not a function of distance from the contact. Therefore, garnet–nepheline syenite and pseudoleucite syenite from Diamond Jo quarry were probably not metasomatized at the time of intrusion of the Diamond Jo nepheline syenite.

Alkali syenite 83-51 underwent late-stage sodic metasomatism distinct from that of Diamond Jo nepheline syenite. Albite rims formed on K-feldspar, natrolite is absent and there is no evidence of late-stage Cl enrichment. Alkali syenite is enriched in Si relative to the other syenites and falls off the trends defined by them (Fig. 2). Contamination by country rock is one possible source of Si enrichment, but no consistent chemical relationship be-

tween metasomatized Stanley Shale (Flohr and Ross, unpubl. data) and alkali syenite, with which the shale is in contact, is found. Alkali syenite probably represents the intrusion of a more evolved magma than the parent magma of Diamond Jo nepheline syenite.

Geochemistry

Diamond Jo nepheline syenite and the other more felsic syenites have slight to moderate negative Eu anomalies (Fig. 3), suggesting fractionation of plagioclase. Sr, however, which would substitute for Ca in plagioclase and/or K-feldspar (Rankama and Sahama, 1950), is an incompatible element (Fig. 4a) indicating that fractionation of feldspar was not important. Both apatite and sphene have relatively high mineral/melt distribution coefficients for Eu (Henderson, 1984) and fractionation of one or both of these minerals, rather than plagioclase, may be responsible for the negative Eu anomalies observed.

Abundant garnet and clinopyroxene in garnet–nepheline syenite and relatively mafic pseudoleucite syenite control the shapes of the REE patterns of these rocks. Both of these minerals, especially the garnet, have high distribution coefficients for the HREE (Schnetzler and Philpotts, 1970). Melanite garnet also has a preference for Sm and Eu relative to the LREE (Mitchell and Brunfelt, 1975). Mitchell and Brunfelt (1975) also observed that the REE concentrations increased and the REE patterns became progressively flatter as the abundance of melanite in their ijolites increased. We conclude that the relatively flat MREE to HREE patterns of the garnet–nepheline syenites and two pseudoleucite syenites from Magnet Cove (Fig. 3b, c) are the result of abundant melanite in the rocks. A positive correlation between abundance of melanite garnet and HREE concentration was also found by Flohr and Ross (1989) in ijolite xenoliths from the Diamond Jo quarry.

The compatible behavior of Zr, Ti, V and P is explained by the early crystallization of several minerals. Early crystallization of perovskite, Ti-bearing pyroxene, Type I magnetite and melanite controlled the compatible behavior of Ti. Melanite also contains significant amounts of Zr and V (Table 5). Early crystallization of apatite in the garnet–nepheline syenites controlled the compatible behaviour of P.

Mineralogy

Pyroxenes. Numerous other investigators have considered the importance of pyroxene crystallization trends in alkaline rocks. The different trends observed and the point at which Na and Fe^{3+} enrichment occurs reflect characteristics of the parent magma, such as Fe^{3+}/Fe^{2+}, f_{O_2} and peralkalinity (e.g., Woolley and Platt, 1988).

The relatively early development of Na-enrichment in pyroxene from nepheline syenite 84-20 (Fig. 8f) may be the result of Na-metasomatism during the intrusion of the Na-rich, aegirine- and natrolite-bearing pegmatite with which it is in contact. The extremely Fe-rich pyroxenes from Diamond Jo nepheline syenite reflect the highly evolved, Mg-poor bulk composition of the syenite magma. Trends of pyroxenes from sphene–nepheline syenite 86-59 and nepheline syenite 85-14B (Fig. 11) do not show any significant Na enrichment, indicating low Na activity, as may be expected from miaskitic nepheline syenites.

A variety of pyroxene trends have been reported in the literature. [Other authors may have calculated Fe^{3+} by methods different from that used in

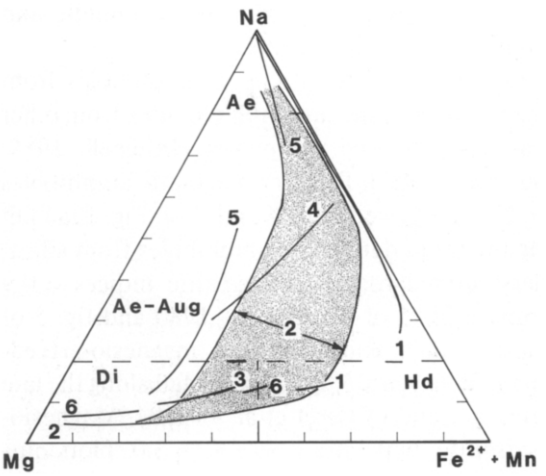

Fig. 11. Generalized crystallization trends of clinopyroxenes plotted in Fig. 8: *1*–Diamond Jo nepheline syenite; *2*–broad trend includes garnet–nepheline syenite, pseudoleucite syenite, the primary part of the alkali syenite trend and miscellaneous nepheline syenites 86-62B and 86-64; *3*–sphene–nepheline syenite; *4*, *5* and *6*–trends defined by miscellaneous nepheline syenites 85-17, 84-20, and 85-14B, respectively. Trend *5* is composed of a low-Na and a high-Na segment from the nepheline syenite and pegmatite, respectively, from 84-20. Abbreviations for clinopyroxene fields are as defined for Fig. 8a.

this study; recalculation of their reported representative analyses suggests that their trend lines are only slightly shifted on the Na–Mg–(Fe^{2+}+Mn) plot and general comparisons with our data are thus possible.] The pyroxene trend from Diamond Jo nepheline syenite (Fig. 11) is similar to the Pantellerite trend (Nicholls and Carmichael, 1969); such narrow trends are typical. The broad garnet–nepheline syenite trend (Figs. 8b, 11) overlaps trends reported from other syenites, such as those from South Qoroq (Stephenson, 1972) and is unusual (e.g., Woolley and Platt, 1988). The wide range of pyroxene compositions and discontinuously zoned grains found in garnet–nepheline syenite on the scale of a thin section indicate that disequilibrium conditions existed in the magma. Perturbations in the crystallizing magma, such as incorporation of mafic segregations, may be responsible for the wide range of zoning trends that make up the composite pyroxene trend found in the garnet–nepheline syenite.

The zoning trends of individual pyroxene grains are all normal and reverse zoning of successive overgrowths is not observed. There is no evidence that mixing between two different magmas caused the discontinuous zoning as documented by O'Brien et al. (1988) in pyroxenes from mixed minette and phonolite–shonkinite magmas.

Amphiboles. Compositions of amphiboles from Magnet Cove syenites are similar to those from other silica-undersaturated complexes (Mitchell, 1989; Giret et al., 1980). Primary magmatic amphiboles from Magnet Cove (Table 9, no. 1–4; Fig. 12a) fall along the trend defined by amphiboles from silica-undersaturated rocks with agpaitic indices <0.9 (compare fig. 5 of Giret et al., 1980 and fig. 5 of Bédard, 1988). Richterite and magnesio-arfvedsonite (Table 9, no. 5, 6; Fig. 12b) fall along the late magmatic trend of Giret et al. (1980). Magnesio-arfvedsonite, with (Ca+Na+K)>3.0, plots outside the arfvedsonite field, however. Ross (1984) proposed that arfvedsonite from an alkali syenite similar to 83-51 with (Ca+Na+K)>3.0 and containing (100) lamellae of aegirine, may indicate the existence of a precursor mixed-chain pyribole. Such (100) lamellae of aegirine are not observed in arfvedsonite in 83-51 on a microscopic scale, but the excess (Ca+Na+K) indicated by microprobe analyses (Table 9, no. 6) suggests that such lamellae may be present. High-resolution transmission-

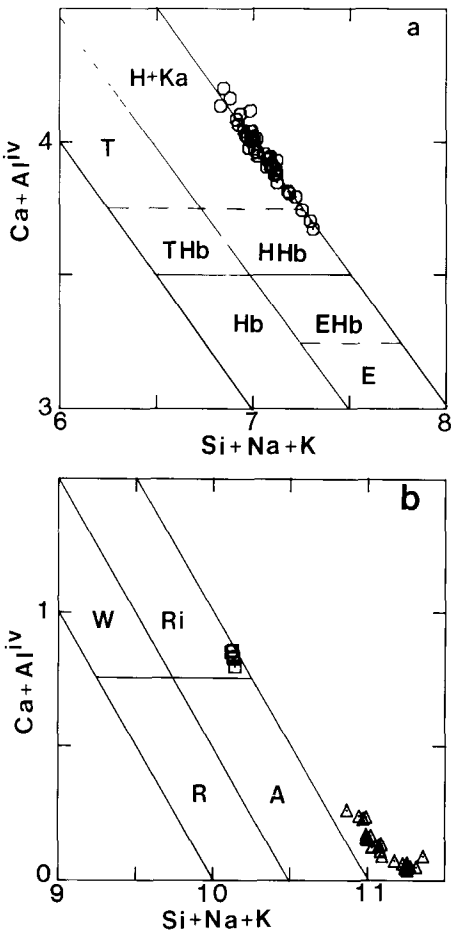

Fig. 12. Electron microprobe analyses of amphiboles (cations) plotted in the system (Ca+Al^{iv}) vs (Si+Na+K) after Giret et al. (1980). (a) Amphiboles from sphene–nepheline syenite 86-59 and nepheline syenite 85-14B define a primary magmatic trend. (b) Analyses of some late magmatic amphiboles (squares) from alkali syenite 83-51 fall within the richterite field, whereas arfvedsonite analyses (triangles), with excess (Ca+Na+K) lie outside the arfvedsonite field. Composition fields are from Giret et al. (1980) and abbreviations are as follows: *H*, hastingsite; *Ka*, kaersutite; *T*, tschermakite; *THb*, tschermakitic hornblende; *HHb*, hastingsitic hornblende; *Hb*, hornblende; *EHb*, edenitic hornblende; *E*, edenite; *Ri*, richterite; *W*, winchite; *R*, riebeckite; *A*, arfvedsonite.

electron microscopy is required to resolve this question.

In amphiboles from sphene–nepheline syenite, there is no significant change in K and Na, a slight decrease in Ca and Al, a decrease in Mg, Ti and F and an increase in Fe^{2+} and Fe^{3+} from core to rim. Giret et al. (1980) and Bédard (1988) suggested that such zoning trends indicate that Mg for Fe^{2+}

and $(Ti^{4+}+O^{2-})$ for $(Fe^{3+}+OH^{-})$ are the most important substitution mechanisms.

Micas. Mn-rich biotite (Table 6, no. 1) is unusual in igneous rocks (Deer et al., 1962) but has been reported from other syenites. Woolley and Platt (1988) reported biotite with as much as 0.826 atoms of Mn per 22 anions from syenites from the Junguni intrusion and Nash and Wilkinson (1970) reported annite with as much as 45% manganphyllite component from syenite from the Shonkin Sag laccolith, Montana.

Feldspars. Feldspars from Magnet Cove syenites are, on the whole, K- and Ba-rich. Sodic perthitic alkali feldspars are uncommon (Fig. 7). K-feldspar from syenites from other complexes generally contain <2 wt.% BaO, whereas K-feldspar from potassic volcanic rocks shows considerable Ba enrichment (Smith and Brown, 1988). The zoning trends observed in the Magnet Cove feldspars, with Ba decreasing from core to rim, are like those observed in Ba-bearing feldspar from minettes (LeCheminant et al., 1987) and in megacrysts from granites (Mehnert and Busch, 1981).

The perthitic intergrowth of two Ba-rich feldspars (Fig. 10b, c) indicates subsolidus unmixing from an original single Ba-rich feldspar, with subsequent crystallization of another relatively low-Ba feldspar, represented by the one-phase rim. Exsolution of Ba-K feldspars has been reported (Nakano, 1979; see also summary by Smith and Brown, 1988), but composition pairs like those described here have apparently not been previously observed.

Replacement of andesine by K-feldspar, as found in sphene–nepheline syenite, has been reported from alkaline rocks from other localities, e.g., in augite syenite from Ilimaussaq (Larsen, 1981), larvikites from the Motzfeldt Centre, Greenland (Jones and Larsen, 1985) and olivine syenite from Granite Mountain, Arkansas (Morris, 1986). Morris (1986) concluded that the K-feldspar formed during a metasomatic event, but the source of the metasomatic fluid was not identified.

No other textural evidence for metasomatism, such as late-stage replacement intergrowths as observed in Diamond Jo nepheline syenite and garnet–nepheline syenite, is found in the sphene–nepheline syenite. Thus replacement of plagioclase by K-feldspar in the sphene–nepheline syenite is the result of progressive crystallization and not metasomatism.

Mafic segregations

Mineral compositions in the mafic segregations that are found in garnet–nepheline syenite are like the mineral compositions in the host rock, indicating that the segregations and their host crystallized from the same magma. No reaction zone or quenched margin is found between a segregation and its host syenite, indicating that the two bodies were in or close to thermal equilibrium when the segregation was incorporated into the magma. The segregations are probably cognate xenoliths that represents dense fractions of the magma that either were sinking or had crystallized along the walls of the magma chamber and became entrained in the ascending, slightly less dense, magma.

Amphibole-rich mafic segregations in sphene–nepheline syenite are also identified as cognate xenoliths. The cores of amphiboles in the segregations are more Mg-rich than cores of amphiboles in the surrounding syenite, indicating crystallization from a slightly less evolved magma than their host. The rims of amphiboles in the segregations are, however, compositionally similar to the cores of amphibole phenocrysts in the surrounding syenite. Compositions of other minerals in the segregations are also like those of the host, strongly indicating a genetic relationship.

Conditions of formation

Erickson and Blade (1963) concluded that the intrusive rocks of Magnet Cove were emplaced at relatively shallow depths after explosive volcanic activity. Magnet Cove has been extensively eroded and very little field evidence remains for extrusive volcanic activity (Ross, 1941; Erickson and Blade, 1963) that is so typical of many of the carbonatite–nephelinite complexes of Africa (Le Bas, 1977). Thus, the exposed rocks of Magnet Cove represent only the intrusive phases of an ancient carbonatite–nephelinite complex. No stratigraphic control is available for calculation of overburden, but fluid inclusion data from carbonatite (Nesbitt and Kelly, 1977) and the model of Hendricks (1988), developed from gravity and magnetic data, are consistent with relatively shallow emplacement of the intrusive rocks. Evidence from other alkaline complexes (e.g., Platt and Woolley, 1986) indicate that syenites in such complexes were emplaced at

relatively shallow depths at pressures of about 1–2 kbar.

Mineral assemblages and compositions also indicate formation of the syenites at low pressure. The coexistence of sodalite, nepheline, and perthitic feldspar in sphene–nepheline syenite indicates a low pressure range of ~1.6–2.75 kbar (Wellman, 1970). The Fe content of richterite in alkali syenite 83-51 (Table 9, no. 6) indicates an upper thermal stability of ~950°C at an f_{O_2} equivalent to the fayalite–magnetite–quartz (FMQ) buffer and low pressure (Charles, 1975). Fluorine substitution for OH may extend the stability of amphiboles (Ernst, 1968; Gilbert et al., 1982) to higher temperature, however.

Amphibole, a common accessory phase in alkaline rocks, is not present in Diamond Jo nepheline syenite, garnet–nepheline syenite, or pseudoleucite syenite. Crystallization of aegirine rather than alkali amphibole at low temperatures indicates an Na-rich environment and high f_{O_2}, above the FMQ buffer (e.g., Ernst, 1968; Stephenson and Upton, 1982) and low a_{H_2O}. The coexistence of ilmenite and aegirine and lack of aenigmatite in pegmatitic segregations also indicates that f_{O_2} was above the FMQ buffer (Marsh, 1975) during late-stage, volatile-rich crystallization. The effect of Mn substitution for Fe^{2+} on the stability of ilmenite is not certain under these conditions. The presence of magnetite throughout the suite of syenites and lack of olivine in even the least evolved syenites indicates that relatively high f_{O_2} prevailed throughout the crystallization history of these rocks.

Experimental data summarized on the composite diagram of Gilbert et al. (1982; their fig. 22) at conditions of the FMQ buffer suggest that amphibole from sphene-nepheline syenite crystallized under a wide range of temperatures. The upper stability of pargasite at low P of ~1.5 kbar is ~1050°C, whereas ferroan pargasite and magnesian hastingsite are stable below ~625–650°C. The range of crystallization temperature may not be this great if f_{O_2} changed as crystallization progressed; for example, at $P=1.5$ kbar and at the f_{O_2} of the wüstite–magnetite buffer, the stability fo ferroan pargasite and magnesian hastingsite is increased to ~850°C and ~900°C, respectively. Magnetite, abundant sphene, which occurs in mafic segregations, as inclusions in amphibole, and as a groundmass phase and lack of perovskite indicate that f_{O_2} was above the FMQ buffer and below the magnetite-hematite buffer throughout the crystallization of the rock.

Compositions of nepheline fall within the Morozewicz–Buerger convergence field of plutonic nepheline, implying temperatures of ~500°C (Hamilton, 1961) for reequilibration or crystallization. Textural relationships indicate that nepheline is a primary magmatic phase, so these temperatures are those of final reequilibration.

Conclusions

Whole-rock major-, minor- and trace-element data and pyroxene zoning trends indicate that syenites from Magnet Cove were derived from at least four different magmas. Mineral compositions indicate crystallization took place at an f_{O_2} at or above the FMQ buffer at relatively low pressure, <3 kbar. Temperatures of crystallization are not well constrained, but the coexistence of pargasite and hastingsite in sphene–nepheline syenite indicate a temperature range of several hundred degrees for the crystallization of this rock.

The compatible behavior of Ti, V, Zr and P in garnet–nepheline syenites with progressive differentiation is explained by early crystallization of such phases as perovskite, apatite, magnetite and garnet. Evidence for mobilization of minor elements, such as Mn, Ti, V and Zr, is found on a very local scale in Diamond Jo nepheline syenite, garnet–nepheline syenite and pseudoleucite syenite. F and/or Cl may have played a role in the mobilization processes.

Acknowledgments

Henry deLinde (Mabelvale, Arkansas), owner of the Diamond Jo quarry, kindly granted access to his property. Mike Howard (Arkansas Geological Commission) and Don Owens (University of Arkansas, Little Rock) helped to collect samples. Mike Howard also provided guidance in locating sampling sites within the complex. Ted Armbrustmacher (U.S.G.S., Denver) provided the portable drill used to obtain core samples and helped to collect samples. G. Wandless, J. Mee, M. Doughten, J. Evans, J. Taggert, A. Bartel, E. Robb, E. Brandt, H. Christie, J. Sharkey, L. Jackson, H. Smith, C. Skeen, H. Kirschenbaum, R. Moore, M. Kavulak, J. Marinenko and N. Rait (U.S.G.S.) provided

whole-rock analyses. Jim McGee (U.S.G.S.) gave advice on selection of electron microprobe standards. We thank Elaine S. McGee and Odette B. James for constructive reviews of an earlier version of this paper and Alan R. Woolley for his comments. This work was funded by the Strategic and Critical Minerals and Development of Assessment Techniques Programs of the U.S.G.S.

References

Bédard, J.H., 1988. Comparative amphibole chemistry of the Monteregian and White Mountain alkaline suites, and the origin of amphibole megacrysts in alkali basalts and lamprophyres. Mineral. Mag., 52: 91–103.

Charles, R.W., 1975. The phase equilibrium of richterite and ferrorichterite. Am. Mineral., 60: 367–374.

Currie, K.L., Eby, G.N. and Gittins, J., 1986. The petrology of the Mont Saint Hilaire complex, southern Quebec: An alkaline gabbro–peralkaline syenite association. Lithos, 19: 65–81.

Deer, W.A., Howie, R.A. and Zussman, J., 1962. Rock Forming Minerals, Vol. 3, Sheet Silicate. Longman, New York, 270 pp.

Deer, W.A., Howie, R.A. and Zussman, J., 1963. Rock Forming Minerals, Vol. 4, Framework Silicates. Longman, New York, 435 pp.

Eby, G.N., 1987. Fission-track geochronology of the Arkansas alkaline province. U.S. Geol. Surv. Open-File Rep. 87-0287, 14 pp.

Erickson, R.L. and Blade, L.V., 1963. Geochemistry and petrology of the alkalic igneous complex at Magnet Cove, Arkansas. U.S. Geol. Surv. Prof. Pap., 425, 95 pp.

Ernst, W.G., 1968. Amphiboles. Springer, New York, 125 pp.

Flohr, M.J.K. and Ross, M., 1985. Nepheline syenite, quartz syenite, and ijolite from the Diamond Jo quarry, Magnet Cove Arkansas. In: R.C. Morris and E.D. Mullen (Editors), Alkalic Rocks and Carboniferous Sandstones, Ouachita Mountains: New Perspectives. Guide. GSA Reg. Meet., Fayetteville, Arkansas, April 16–18, 1985, pp. 63–75.

Flohr, M.J.K. and Ross, M., 1989. Alkaline igneous rocks of Magnet Cove, Arkansas: Metasomatized ijolite xenoliths from Diamond Jo quarry. Am. Mineral., 74: 113–131.

Gilbert, M.C., Helz, R.T., Popp, R.K. and Spear, F.S., 1982. Experimental studies of amphibole stability. In: D.R. Veblen and P.H. Ribbe (Editors), Amphiboles: Petrology and experimental phase relationships. Mineral. Soc. Am. Re. Mineral., 9B, 229–353.

Giret, A., Bonin, B. and Leger, J.-M., 1980. Amphibole compositional trends in oversaturated and undersaturated alkaline plutonic ring-complexes. Can. Mineral., 18: 481–495.

Hamilton, D.L., 1961. Nepheline as crystallization temperature indicators. J. Geol., 69: 321–329.

Henderson, P., 1984. General geochemical properties and abundances of the rare earth elements. In: P. Henderson (Editor), Rare Earth Element Geochemistry. Elsevier, Amsterdam, pp. 1–32.

Hendricks, J.D., 1988. Bouguer gravity of Arkansas. U.S. Geol. Surv. Prof. Pap., 1474, 31 pp.

Ilton, E.S. and Eugster, H.P., 1989. Base metal exchange between magnetite and a chloride-rich hydrothermal fluid. Geochim. Cosmochim. Acta, 53: 291–301.

Jones, A.P. and Larsen, L.M., 1985. Geochemistry and REE minerals of nepheline syenites from the Motzfeldt Centre, South Greenland. Am. Mineral., 70: 1087–1100.

Kogarko, L.N., 1974. Role of volatiles. In: H. Sørensen (Editor), The Alkaline Rocks. Wiley, New York, pp. 474–487.

Kogarko, L.N., 1987. Alkaline rocks of the eastern part of the Baltic shield (Kola Peninsula). In: J.G. Fitton and B.G.J. Upton (Editors), Alkaline igneous rocks. Geol. Soc. Spec. Publ., 30. Blackwell Sci. Publ., London, 531–544.

Koster van Groos, A.F. and Wyllie, P.J., 1968. Melting relationships in the system $NaAlSi_3O_8$–NaF-H_2O to 4 kilobars pressure. J. Geol., 76: 50–70.

Koster van Groos, A.F. and Wyllie, P.J., 1969. Melting relationships in the system $NaAlSi_3O_8$–NaCl–H_2O at one kilobar pressure, with petrologic applications. J. Geol., 77: 581–605.

Larsen, L.M., 1981. Chemistry of feldspars in the Ilimaussaq augite syenite with additional data on some other minerals. Rapp. Grønlands Geol. Unders., 103: 31–37.

Le Bas, M.J., 1977. Carbonatite–nephelinite volcanism. Wiley, New York, 347 pp.

LeCheminant, A.N., Miller, A.R. and LeCheminant, G.M., 1987. Early Proterozoic alkaline igneous rocks, District of Keewatin, Canada: Petrogenesis and mineralization. In: T.C. Pharaoh, R.D. Beckinsale and D. Rickard (Editors), Geochemistry and Mineralization of Proterozoic Volcanic Suites. Geol. Soc. Spec. Publ., 33. Blackwell Sci. Publ., London, pp. 219–240.

Marsh, J.S., 1975. Aenigmatite stability in silica-undersaturated rocks. Contrib. Mineral. Petrol., 50: 135–144.

Mehnert, K.R. and Büsch, W., 1981. The Ba content of K-feldspar megacrysts in granites: A criterion for their formation. N. Jahrb. Mineral. Abh., 140: 221–252.

Mitchell, R.H., 1989. Compositional variation of amphiboles in alkaline rocks (abs.). 28th Int. Geol. Congr. Washington, D.C., U.S.A., July 9–19, 1989, 2: 445–446.

Mitchell, R.H. and Brunfelt, A.O., 1975. Rare earth element geochemistry of the Fen alkaline complex, Norway. Contrib. Mineral. Petrol., 52: 247–259.

Morimoto, N., 1988. Nomenclature of pyroxenes. Am. Mineral., 73: 1123–1133.

Morris, E.M., 1986. The syenites of Granite Mountain, Arkansas: A progress report. In: C.G. Stone and B. Haley (Editors), Sedimentary and igneous rocks of the Ouachita Mountains: A guidebook with contributed papers. Arkansas Geol. Comm., no. 86-3, pp. 91–98.

Nakano, S., 1979. Intergrowth of barium microcline, hyalophane and albite in the barium-containing alkali feldspar from the Noda-Tamagawa mine, Iwate Prefecture, Japan. Mineral. J. Japan, 9: 409–416.

Nash, W.P. and Wilkinson, J.F.G., 1970. Shonkin Sag laccolith, Montana: I. Mafic minerals and estimates of temper-

ature, pressure, oxygen fugacity and silica activity. Contrib. Mineral. Petrol., 25: 241–269.

Nesbitt, B.E. and Kelly, W.C., 1977. Magmatic and hydrothermal inclusions in carbonatite of the Magnet Cove complex, Arkansas. Contrib. Mineral. Petrol., 63: 271–294.

Nicholls, J. and Carmichael, J.S.E., 1969. Peralkaline acid liquids: A petrological study. Contrib. Mineral. Petrol., 20: 268–294.

O'Brien, H.E., Irving, A.J. and McCallum, I.S., 1988. Complex zoning and resorption of phenocrysts in mixed potassic mafic magmas of the Highwood Mountains, Montana. Am. Mineral., 73: 1007–1024.

Owens, D.R. and Howard, J.M., 1991. Bedrock mapping and geology of the Diamond Jo quarry. Arkansas Geol. Comm. Open-File Rep., in press.

Platt, R.G. and Woolley, A.R., 1986. The mafic mineralogy of the peralkaline syenites and granites of the Mulanje complex, Malawi. Mineral. Mag., 50: 85–99.

Rankama, K. and Sahama, G., 1950. Geochemistry. University of Chicago Press, Chicago, 912 pp.

Ross, C.S., 1941. Occurrence and origin of the titanium deposits of Nelson and Amherst Counties, Virginia. U.S. Geol. Surv. Prof. Pap., 198, 59 pp.

Ross, M., 1984. Ultra-alkalic arfvedsonite and associated richterite, acmite, and aegirine-augite in quartz syenite, Magnet Cove alkalic igneous complex, Arkansas (abs.). EOS (Trans. Am. Geophys. Union), 65: 293.

Schnetzler, C.C. and Philpotts, J.A., 1970. Partition coefficients of rare-earth elements between igneous matrix mineral and rock-forming mineral phenocrysts–II. Geochim. Cosmochim. Acta, 34: 331–340.

Smith, J.V. and Brown, W.L., 1988. Feldspar Minerals, Vol. 1. Springer, Heidelberg, 828 pp.

Sørensen, H., 1974. The Alkaline Rocks. Wiley, New York, 622 pp.

Stephenson, D., 1972. Alkali clinopyroxenes from nepheline syenites of the South Qoroq Centre, south Greenland. Lithos, 5: 187–201.

Stephenson, D. and Upton, B.G.J., 1982. Ferromagnesian silicates in a differentiated alkaline complex: Kungnat Fjeld, South Greenland. Mineral. Mag., 46: 283–300.

Tilley, C.E., 1954. Nepheline–alkali feldspar paragenesis. Am. J. Sci., 252: 65–75.

Vlasov, K.A., Kuz'menko, M.Z. and Es'kova, E.M., 1966. The Lovozero alkali massif. Hafner, New York, 627 pp.

Wellman, T.R., 1970. The stability of sodalite in a synthetic syenite plus aqueous chloride fluid system. J. Petrol., 11: 49–71.

Williams, J.F., 1891. The igneous rocks of Arkansas. Arkansas Geol. Surv. Annu. Rep. 1890, 2: 1–391, 429–457.

Woolley, A.R. and Platt, R.G., 1988. The peralkaline nepheline syenites of the Junguni intrusion, Chilwa province, Malawi. Mineral. Mag., 52: 425–433.

Zartman, R.E., 1977. Geochronology of some alkalic provinces in eastern and central United States. Annu. Rev. Earth Planet. Sci., 5: 257–286.